united nations
educational, scientific
and cultural
organization

international atomic
energy agency

the
**abdus salam**
international centre for theoretical physics

SMR 1302 - 6

**WINTER SCHOOL ON LASER SPECTROSCOPY AND APPLICATIONS**

**19 February - 2 March 2001**

# *MODERN SPECTROSCOPY AND INSTRUMENTATION*

## *Part II*

Wolfgang DEMTRÖDER
Univ. Kaiserslautern - Fachbereich Physik
67653 Kaiserslautern - Germany

***These are preliminary lecture notes, intended only for distribution to participants.***

strada costiera, 11 - 34014 trieste italy - tel. +39 040224011 | fax +39 040224163 - sci_info@ictp.trieste.it - www.ictp.trieste.it

Lectures II
on Laser Spectroscopy.
W. Demtröder
Trieste Winterschool 2001.

# 6. Doppler-Limited Absorption and Fluorescence Spectroscopy with Lasers

After having presented in the previous chapter the different realizations of tunable lasers, we now discuss their applications in absorption and fluorescence spectroscopy. At first those methods where the spectral resolution is limited by the Doppler width of the molecular absorption lines will be treated. This limit can in fact be reached if the laser linewidth is small compared with the Doppler width. In several examples, such as optical pumping or laser-induced fluorescence spectroscopy, multimode lasers may be employed, although in most cases single-mode lasers will be superior. In general, however, these lasers may not necessarily be frequency stabilized as long as the frequency jitter is small compared with the absorption linewidth. We compare several detection techniques of molecular absorption with regard to their sensitivity and their feasibility in the different spectral regions. Some examples illustrate the methods to give the reader a feeling of what has been achieved. After the discussion of the "Doppler-limited spectroscopy", Chaps.7-10 give an extensive treatment of various techniques which allow sub-Doppler spectroscopy.

## 6.1 Advantages of Lasers in Spectroscopy

In order to illustrate the advantages of absorption spectroscopy with tunable lasers, at first we compare it with the conventional absorption spectroscopy which uses incoherent radiation sources. Figure 6.1 presents schematic diagrams for both methods.

In classical absorption spectroscopy, radiation sources with a *broad emission continuum* are preferred (e.g., high-pressure Hg arcs, Xe flash lamps, etc.). The radiation is collimated by the lens $L_1$ and passes through the absorption cell. Behind a dispersing instrument for wavelength selection (spectrometer or interferometer) the intensity $I_T(\lambda)$ of the transmitted light is measured as a function of the wavelength $\lambda$ (Fig.6.1a). By comparison with the reference beam $I_R(\lambda)$ (which can be realized, for instance, by shifting the absorption cell alternatively out of the light beam) the absorption spectrum

$$I_A(\lambda) = a[I_0(\lambda) - I_T(\lambda)] = a[bI_R(\lambda) - I_T(\lambda)]$$

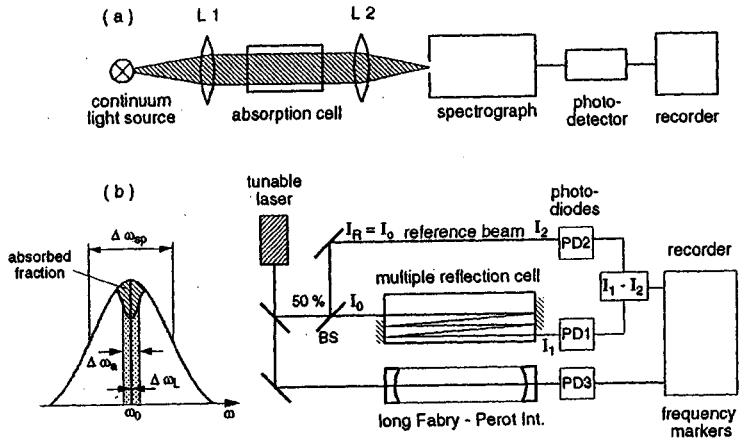


**Fig.6.1.** Comparison between absorption spectroscopy with a broadband incoherent source (a) and with a tunable single-mode laser (b)

can be obtained, where the constants a and b take into account wavelength-independent losses of $I_R$ and $I_T$ (e.g., reflections of the cell walls).

The *spectral resolution* is generally limited by the resolving power of the dispersing spectrometer. Only with large and expensive instruments (e.g., Fourier spectrometers) may the Doppler limit be reached [6.1].

The *detection sensitivity* of the experimental arrangement is defined by the minimum absorbed power which can still be detected. In most cases it is limited by the detector noise and by intensity fluctuations of the radiation source. Generally the limit of the detectable absorption is reached at relative absorptions $\Delta I/I \geq 10^{-4}-10^{-5}$. This limit can be pushed further down only in favorable cases by using special sources and lock-in detection or signal-averaging techniques.

Contrary to radiation sources with broad emission continua used in conventional spectroscopy, tunable lasers offer radiation sources in the spectral range from the UV to the IR with extremely narrow bandwidths and with spectral power densities which may exceed those of incoherent light sources by many orders of magnitude (Sects.5.7,8).

In several regards laser absorption spectroscopy corresponds to microwave spectroscopy where clystrons or carcinotrons instead of lasers represent tunable coherent radiation sources. Laser spectroscopy transfers many of the techniques and advantages of microwave spectroscopy to the infrared, visible, and ultraviolet spectral ranges.

The advantages of absorption spectroscopy with tunable lasers may be summarized as follows:

- No monochromator is needed since the absorption coefficient $\alpha(\omega)$ and its frequency dependence can be directly measured from the difference $\Delta I(\omega) = a[I_R(\omega)-I_T(\omega)]$ between the intensities of the reference beam with $I_R = I_2$ and transmitted beam $T_T = I_1$ (Fig.6.1b). The spectral resolution is



higher than in conventional spectroscopy. With tunable single-mode lasers it is only limited by the linewdiths of the absorbing molecular transitions. Using Doppler-free techniques (Chaps.7-10), even sub-Doppler resolution can be achieved.

- Because of the high spectral power density of many lasers, the detector noise is generally negligible. Intensity fluctuations of the laser which limit the detection sensitivity, may essentially be suppressed by intensity stabilization (Sect.5.4). This furthermore increases the signal-to-noise ratio and therefore enhances the sensitivity.

- The detection sensitivity increases with increasing spectral resolution $\omega/\Delta\omega$ as long as $\Delta\omega$ is still larger than the linewidth $\delta\omega$ of the absorption line. This can be seen as follows.

The relative intensity attenuation per absorption path length x = 1 cm on the transition with center frequency $\omega_0$ is for small absorption $\alpha x << 1$

$$\Delta I/I = \int_{\omega_0-\frac{1}{2}\Delta\omega}^{\omega_0+\frac{1}{2}\Delta\omega} \alpha(\omega)\, I(\omega)\, d\omega \Big/ \int_{\omega_0-\frac{1}{2}\delta\omega}^{\omega_0+\frac{1}{2}\delta\omega} I(\omega)\, d\omega\,. \tag{6.1}$$

If $I(\omega)$ does not change much within the interval $\Delta\omega$ we can write

$$\int_{\omega_0-\frac{1}{2}\Delta\omega}^{\omega_0+\frac{1}{2}\Delta\omega} I(\omega)\, d\omega = \bar{I}\,\Delta\omega \quad \text{and} \quad \int\alpha(\omega)\, I(\omega)\, d\omega = \bar{I}\int\alpha(\omega)\, d\omega\,.$$

This yields

$$\frac{\Delta I}{I} = \frac{1}{\Delta\omega}\int_{\omega_0-\frac{1}{2}\delta\omega}^{\omega_0+\frac{1}{2}\delta\omega} \alpha(\omega)\, d\omega \simeq \bar{\alpha}\,\frac{\delta\omega}{\Delta\omega} \quad \text{for} \quad \Delta\omega > \delta\omega\,. \tag{6.2}$$

---

**Example 6.1**

The spectral resolution of a 1-m spectrograph is about 0.1 Å, which corresponds at $\lambda$ = 500 nm to $\Delta\omega = 2\pi\cdot 12$ GHz. The Doppler width of gas molecules with M = 30 at T = 300 K is, according to (3.43) $\delta\omega \simeq 2\pi\cdot 1$ GHz. With a single-mode laser the value of $\delta\omega$ becomes smaller than $\Delta\omega$ and the observable signal $\Delta I/I$ becomes 12 times larger.

---

- Because of the good collimation of a laser beam, long absorption paths can be realized by multiple reflection back and forth through the multiple-path absorption cell. Disturbing reflections from cell walls or windows which may influence the measurements can essentially be avoided (for ex-

ample, by using Brewster end windows). Such long absorption paths enable measurements of transitions even with small absorption coefficients. Furthermore pressure broadening can be reduced by using low gas pressure. This is especially important in the infrared region where the Doppler width is small and the pressure broadening may become the limiting factor for the spectral resolution (Sect.3.3).

---

**Example 6.2**

With an intensity stabilized light source and lock-in detection the minimum relative absorption which may be safely detected, is about $\Delta I/I \geq 10^{-6}$, which yields the minimum measurable absorption coefficient for an absorption pathlength L

$$\alpha \geq \frac{10^{-6}}{L} \frac{\Delta\omega}{\delta\omega} \quad [\mathrm{cm}^{-1}] ,$$

For L = 10 cm and $\delta\omega = 10\Delta\omega$ we obtain $\alpha \geq 10^{-6}$ cm$^{-1}$. With single-mode lasers one may reach $\Delta\omega < \delta\omega$ and L = 10 m which yields a minimum detectable absorption coefficient of $\alpha \geq 10^{-9}$ cm$^{-1}$, i.e. an improvement of a factor of 1000 !

---

- If a small fraction of the laser output is sent through a long Fabry-Perot interferometer with a separation d of the mirrors, the photodetector PD3 receives intensity peaks each time the laser frequency $\nu_L$ is tuned to a transmission maximum at $\nu = \frac{1}{2}mc/d$ (Sects.4.2,4). These peaks serve as accurate wavelength markers which allow one to calibrate the separation of adjacent absorption lines (Fig.6.1). With d = 1 m the frequency separation $\Delta\nu_p$ between successive transmission peaks is $\Delta\nu_p = c/2d = 150$ MHz, corresponding to a wavelength separation of $10^{-4}$ nm at $\lambda = 550$ nm. With a semiconfocal FPI the free spectral range is c/8d, which gives $\Delta\nu_p = 75$ MHz for d = 0.5 m.
- The laser frequency may be stabilized onto the center of an absorption line. With the methods discussed in Sect.4.4 it is possible to measure the wavelength $\lambda_L$ of the laser with an absolute accuracy of $10^{-8}$ or better. This allows determination of the molecular absorption lines with the same accuracy.
- It is possible to tune the laser wavelength very rapidly over a spectral region where molecular absorption lines have to be detected. With electro-optical components, for instance, pulsed dye lasers can be tuned over several wave numbers within a microsecond. This opens new perspectives for spectroscopic investigations of short-lived intermediate radicals in chemical reactions. The capabilities of classical flash photolysis may be considerable extended using such rapidly tunable laser sources.



- An important advantage of absorption spectroscopy [illegible] mode lasers stems from their capabilites to measure line profiles of absorbing molecular transitions with high accuracy. In case of pressure broadening the determination of line profiles allows one to derive information about the interaction potential of the collision partners (Sects.3.3 and 13.1). In plasma physics this technique is widely used to determine electron and ion densities and temperatures.
- In fluorescence spectroscopy and optical pumping experiments, the high intensity of lasers allows an appreciable population in selectively excited states to be achieved which may be comparable to that of the absorbing ground states. The small laser linewidth favors the selectivity of optical excitation and results in favorable cases in the exclusive population of single molecular levels. These advantageous conditions allow one to perform absorption and fluorescence spectroscopy of *excited* states and to transform spectroscopic methods, such as microwave or RF spectroscopy, which has up to now been restricted to electronic ground states, also to excited states.

This brief overview of some advantages of lasers in spectroscopy will be outlined in more detail in the following chapters and several examples will illustrate their relevance.

## 6.2 High-Sensitivity Methods of Absorption Spectroscopy

The general method for measuring absorption spectra is based on the determination of the absorption coefficient $\alpha(\omega)$ from the spectral intensity

$$I_T(\omega) = I_0 \exp[-\alpha(\omega)x] \tag{6.3}$$

which is transmitted through an absorbing path length x. For small absorption $\alpha x << 1$ we can use the approximation $\exp(-\alpha x) \simeq 1-\alpha x$, and (6.3) can be reduced to

$$I_T(\omega) \simeq I_0[1 - \alpha(\omega)x] . \tag{6.4}$$

With the reference intensity $I_R = I_0$, as produced, for example, by a 50% beam splitter with the reflectivity R = 0.5 (Fig.6.1b), one can measure the absorption coefficient

$$\alpha(\omega) = \frac{I_R - I_T(\omega)}{I_R x} \tag{6.5}$$

from the difference $\Delta I = I_R - I_T(\omega)$.

The absorption coefficient $\alpha_{ik}(\omega)$ of the transition $|i\rangle \rightarrow |k\rangle$ with an absorption cross section $\sigma_{ik}$ is determined by the density $N_i$ of absorbing molecules:

$$\alpha_{ik}(\omega) = [N_i - (g_i/g_k)N_k]\sigma_{ik}(\omega) = \Delta N \sigma_{ik}(\omega) . \tag{6.6}$$

If the population $N_k$ is small compared to $N_i$, we obtain from (6.6) for the minimum detectable density $N_i$ over the absorption path length x = L:

$$\boxed{N_i \geq \frac{\Delta I}{I_0 L \sigma_{ik}} .} \tag{6.7}$$

The minimum, still detectable concentration $N_i$ of absorbing molecules is determined by the absorption path length L, the absorption cross section $\sigma_{ik}$, and the minimum detectable, relative intensity change $\Delta I/I_0$ caused by absorption.

*In order to reach a high detection sensitivity for absorbing molecules, $L\sigma_{ik}$ should be large and the minimum detectable value of $\Delta I/I$ as small as possible.*

In the case of very small values of $\alpha x$, this method in which the attenuation of the transmitted light is measured, cannot be very accurate since it has to determine a small difference $I_0 - I_T$ of two large quantities $I_0$ and $I_T$. Small fluctuations of $I_0$ or of the splitting ratio of the beam splitter BS in Fig.6.1b can already severely influence the measurement. Therefore, other techniques have been developed leading to an increase of sensitivity and accuracy of absorption measurements by several orders of magnitude compared to direct absorption measurements. These sensitive detection methods represent remarkable progress, since their sensitivity limits have been pushed from relative absorptions $\Delta\alpha/\alpha \simeq 10^{-5}$ down to about $\Delta\alpha/\alpha \geq 10^{-17}$. We now discuss these different methods in more detail.

### 6.2.1 Frequency Modulation

The first scheme to be treated is based on a frequency modulation of the monochromatic incident wave. It has not been designed specifically for laser spectroscopy but was taken from microwave spectroscopy where it is a standard method. The laser frequency $\omega_L$ is modulated at the modulation frequency f, which tunes $\omega_L$ periodically from $\omega_L$ to $\omega_L + \Delta\omega_L$. When the laser is tuned through the absorption spectrum, the difference $I_T(\omega_L) - I_T(\omega_L + \Delta\omega_L)$ is detected with a lock-in amplifier (phase-sensitive detector) tuned to the modulation frequency (Fig.6.2). If the modulation sweep $\Delta\omega_L$ is sufficiently small, the first term of the Taylor expansion

$$I_T(\omega_L + \Delta\omega_L) - I_T(\omega_L) = \frac{dI_T}{d\omega}\Delta\omega_L + \frac{1}{2!}\frac{d^2 I_T}{d\omega^2}\Delta\omega_L^2 + \ldots \tag{6.8}$$



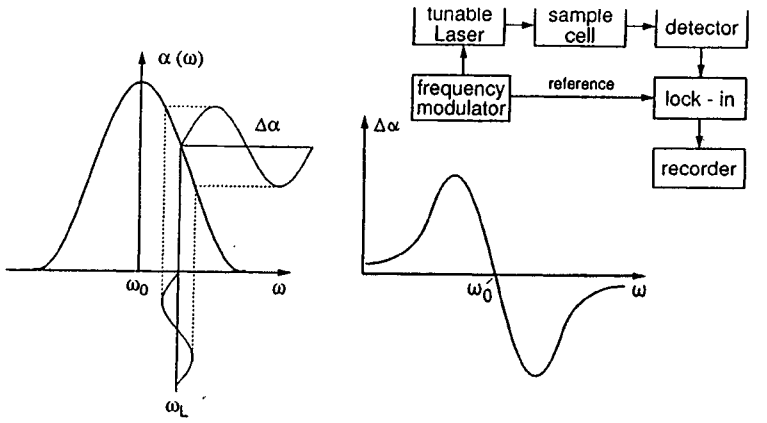


**Fig.6.2.** Absorption spectroscopy with a frequency modulated single-mode laser

is dominant. This term is proportional to the first derivative of the absorption spectrum, as can be seen from (6.5): When $I_R$ is independent of $\omega$ we obtain for the absorption length L

$$\frac{d\alpha(\omega)}{d\omega} = -\frac{1}{I_R L}\frac{dI_T}{d\omega} . \tag{6.9}$$

If the laser frequency

$$\omega_L(t) = \omega_0 + a\sin\Omega t$$

is sinusoidally modulated at a modulation frequency $\Omega$ the Taylor expansion yields

$$I_T(\omega_L) = I_T(\omega_0) + \sum_n \frac{a^n}{n!}\sin^n\Omega t \left(\frac{d^n I_T}{d\omega^n}\right)_{\omega_0} . \tag{6.10}$$

For $\alpha L << 1$ we obtain from (6.4)

$$\left(\frac{d^n I_T}{d\omega^n}\right)_{\omega_0} = -I_0 x \left(\frac{d^n \alpha(\omega)}{d\omega^n}\right)_{\omega_0} .$$

The terms $\sin^n\Omega t$ can be converted into linear functions of $\sin(n\Omega t)$ and $\cos(n\Omega t)$ using known trigonometric formula.

Inserting these relations into (6.10) one finds after rearrangement of the terms the expression

$$\frac{I_T(\omega_L) - I_T(\omega_0)}{I_0} = -aL\left\{\left[\frac{a}{4}\left(\frac{d^2\alpha}{d\omega^2}\right)_{\omega_0} + \frac{a^3}{64}\left(\frac{d^4\alpha}{d\omega^4}\right)_{\omega_0} + \ldots\right]\right.$$

$$+\left[\left(\frac{d\alpha}{d\omega}\right)_{\omega_0} + \frac{a^2}{8}\left(\frac{d^3\alpha}{d\omega^3}\right)_{\omega_0} + \ldots\right]\sin(\Omega t)$$

$$+\left[-\frac{a}{4}\left(\frac{d^2\alpha}{d\omega^2}\right)_{\omega_0} + \frac{a^3}{48}\left(\frac{d^4\alpha}{d\omega^4}\right)_{\omega_0} + \ldots\right]\cos(2\Omega t)$$

$$\left.+\left[-\frac{a^2}{24}\left(\frac{d^3\alpha}{d\omega^3}\right)_{\omega_0} + \frac{a^4}{384}\left(\frac{d^5\alpha}{d\omega^5}\right)_{\omega_0} + \ldots\right]\sin(3\Omega t) + \ldots\right\} .$$

For a sufficiently small modulation amplitude ($a/\omega_0 \ll 1$) the first terms in each bracket are dominant and we obtain for the signal $S(n\Omega)$ behind a lock-in amplifier, tuned to the frequency $n\Omega$ (Fig.6.3):

$$S(n\Omega) = \left(\frac{I_T(\omega_L) - I_T(\omega_0)}{I_0}\right)_{n\Omega} = aL\begin{cases} b_n \sin(n\Omega t) & \text{for } n = 2m+1 \\ c_n \cos(n\Omega t) & \text{for } n = 2m . \end{cases}$$

In particular, the signals for the first three derivatives of the absorption coefficient $\alpha(\omega)$, shown in Fig.6.3, are

$$S(\Omega) = -aL\frac{d\alpha}{d\omega}\sin(\Omega t)$$

$$S(2\Omega) = +\frac{a^2L}{4}\frac{d^2\alpha}{d\omega^2}\cos(2\Omega t) \qquad (6.11)$$

$$S(3\Omega) = +\frac{a^3L}{24}\frac{d^3\alpha}{d\omega^3}\sin(3\Omega t) .$$

The advantage of this "derivative spectroscopy" [6.2] with a frequency modulation of the laser is the possibility for phase-sensitive detection, which restricts the frequency response of the detection system to a narrow frequency interval centered at the modulation frequency $\Omega$. Frequency-independent background absorption from cell windows and background noise due to fluctuations of the laser intensity or of the density of absorbing molecules are essentially reduced. Regarding the signal-to-noise ratio and achievable sensitivity, the *frequency* modulation technique is superior to an *intensity* modulation of the incident radiation. The frequency of a single-mode laser can readily be modulated when an AC voltage is applied to the piezo onto which a resonator mirror is mounted (Sect.5.5).

The technical noise which represents the major limitation decreases with increasing frequency. It is therefore advantageous to choose the modulation frequency as high as possible. For diode lasers this can be achieved by modulation of the diode current. For other lasers, often electro-optical



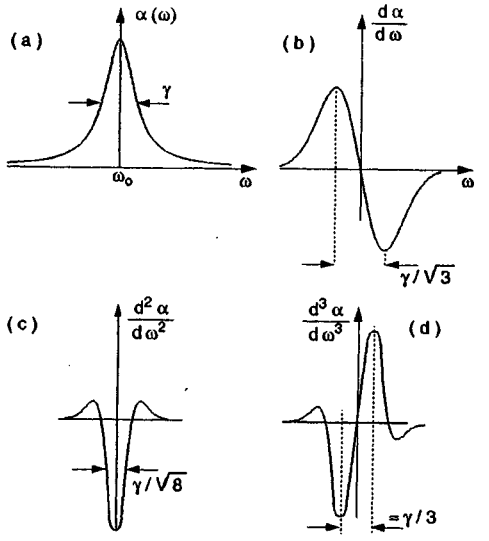


**Fig.6.3.** Lorentzian line profile $\alpha(\omega)$ of halfwidth $\gamma$ (FWHM) (**a**) with first (**b**) second (**c**) and third (**d**) derivatives

modulators outside the laser resonator are used as phase modulators resulting in a frequency modulation of the transmitted laser beam [6.3].

If the modulation frequency $\Omega$ is chosen sufficiently high ($\Omega$ > 1000 MHz) the technical noise may drop below the quantum-noise limit set by the statistical fluctuations of detected photons. In this case the detection limit is mainly due to the quantum limit [6.4].

A new method of high-frequency modulation spectroscopy using low-frequency detection is two-tone frequency-modulation spectroscopy [6.5], where the laser output is phase-modulated in an electro-optic $LiTaO_3$ crystal, which is driven by a high-frequency voltage in the GHz range, that is amplitude-modulated at frequencies in the MHz range. The detector output is fed into a frequency mixer (down converter) and the final signal is received with a lock-in amplifier in the kHz range [6.6.7].

### 6.2.2 Intracavity Absorption

When the absorbing sample is placed inside the laser cavity (Fig.6.4) the detection sensitivity can be enhanced considerably, in favorable cases by several orders of magnitude. Four different effects can be utilized to achieve this "amplified" sensitivity. The first two are based on single-mode operation, the last two on multimode oscillation of the laser.

1) Assume that the reflectivities of the two resonator mirrors are $R_1 = 1$ and $R_2 = 1 - T_2$ (mirror absorption is neglected). At the laser output power

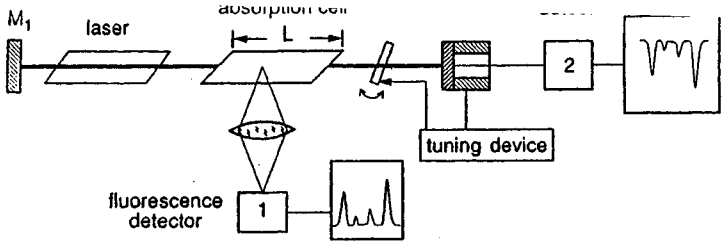


Fig.6.4. Intracavity absorption detected either by monitoring the laser output $P(\omega_L)$ with detector 2 or the laser-induced fluorescence $I_{Fl}(\omega_L)$ with detector 1

$P_{out}$ the power inside the cavity is $P_{int} = qP_{out}$ with $q = 1/T_2$. For $\alpha L << 1$ the power $\Delta P(\omega)$ absorbed at the frequency $\omega$ in the absorption cell (length L) is

$$\Delta P(\omega) = \alpha(\omega) L P_{int} = q\alpha(\omega) L P_{out} \,. \tag{6.12}$$

If the absorbed power can be measured directly, for example through the resulting pressure increase in the absorption cell (Sect.6.3.3) or through the laser-induced fluorescence (Sect.6.3.1), the signal will be q times larger than for the case of single-pass absorption outside the cavity. .

---

**Example 6.3**

With a resonator transmission $T_2 = 0.02$ (a figure which can be readily realized in practice) the enhancement factor becomes $q = 50$, as long as saturation effects can be neglected, and provided the absorption is sufficiently small that it does not noticeably change the laser intensity.

---

This q-fold amplification of the sensitivity can be also understood from the simple fact that a laser photon travels on the average q times back and forth between the resonator mirrors before it leaves the resonator. It therefore has a q-fold chance to be absorbed in the sample.

This sensitivity enhancement in detecting small absorptions has no direct correlation with the gain medium and can be also realized in external passive resonators. If the laser output is mode matched (Sect.5.11) by lenses or mirrors into the fundamental mode of the passive cavity containing the absorbing sample (Fig.6.5), the radiation power inside this cavity is q times larger. The enhancement factor q may become larger, if the internal losses of the cavity can be kept low.

Intracavity absorption cells are particularly advantageous, if the absorption is monitored via the laser-induced fluorescence. Since the radiation field inside the active resonator or inside the mode-matched passive cavity is concentrated within the region of the Gaussian beam (Sect.5.11), the laser-excited fluorescence can be effectively imaged onto the entrance slit



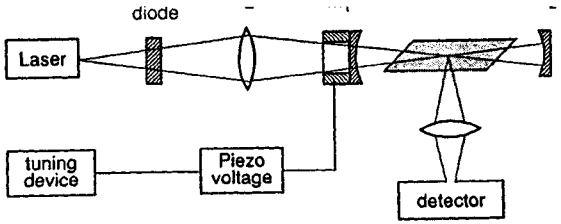


Fig.6.5. Spectroscopy inside an external resonator, which is synchroneously tuned with the laser frequency $\omega_L$

of a spectrometer with a larger efficiency than in the commonly used multipass cells. If minute concentrations of an absorbing component have to be selectively detected in the presence of other constituents with overlapping absorption lines but different fluorescence spectra, the use of a spectrometer for dispersing the fluorescence can solve the problem.

External passive resonators may become advantageous when the absorption cell cannot be placed directly inside the active laser resonator. However, there also exist some drawbacks: The cavity length has to be changed synchroneously with the tunable-laser wavelength, in order to keep the external cavity always in resonance. Furthermore, one has to take care to prevent optical feedback from the passive to the active cavity, which causes a coupling of both cavities with resulting instabilities. This feedback can be avoided by an optical diode (Sect.5.5).

2) Another way of detecting intracavity absorption with a very high sensitivity relies on the dependence of laser output power on absorption losses inside the laser resonator (detector *2* in Fig.6.4). At constant pump power, closely above threshold, minor changes of the intracavity losses may already result in drastic changes of the laser output. In Sect.5.3 we saw that under steady-state conditions the laser ouput power essentially depends on the pump power and reaches the value $P_s$ where the gain factor $G = \exp[-2L_1\alpha_s - \gamma]$ becomes $G = 1$. This implies that the saturated gain $g_s = 2L_1\alpha_s$ of the active medium with the length $L_1$ equals the total losses $\gamma$ per cavity round trip (Sect.5.1).

The saturated gain $g_s = 2L_1\alpha_s$ depends on the intracavity intensity I. According to (3.81) we obtain

$$g_s = \frac{g_0}{1 + I/I_s} = \frac{g_0}{1 + P/P_s} = \gamma \tag{6.13}$$

where $I_s$ is the saturation intensity which decreases $g_0$ to $g_s = g_0/2$ (Sect. 3.6). At a constant pump power the laser power P stabilizes itself at the value where $g_s = \gamma$. This gives with (6.13):

$$P = P_s(g_0/\gamma - 1) \,. \tag{6.14}$$

If small additional losses $\Delta\gamma$ are introduced by ... inside the cavity, the laser power drops to a value $P_\alpha = P - \Delta P$ where

$$\frac{g_0}{1 + P_\alpha/P_s} = \gamma + \Delta\gamma \,. \tag{6.15}$$

From (6.13-15) we obtain for the relative change $\Delta P/P$ of the laser output power by the absorbing sample

$$\frac{\Delta P}{P_s} = \frac{g_0 \Delta\gamma}{\gamma(\gamma + \Delta\gamma)}$$

which can be written with $P_s = P\gamma/(g_0 - \gamma)$ and $\Delta\gamma \ll \gamma$ as

$$\frac{\Delta P}{P} = \frac{g_0}{g_0 - \gamma} \frac{\Delta\gamma}{\gamma + \Delta\gamma} \simeq \frac{g_0}{\gamma} \frac{\Delta\gamma}{g_0 - \gamma} \tag{6.16}$$

where $g_0$ is the unsaturated gain.

Compared with the single-pass absorption of a sample with the absorption coefficient $\alpha$ and the absorption pathlength $L_2$ outside the laser resonator where $\Delta P/P = -\alpha L_2 = -\Delta\gamma$, the intracavity absorption represents a sensitivity enhancement by the factor

$$\boxed{Q = \frac{g_0}{\gamma(g_0 - \gamma)} \,.} \tag{6.17}$$

At pump powers far above threshold the unsaturated gain $g_0$ is large compared to the losses $\gamma$ and (6.17) reduces to

$$Q \simeq 1/\gamma \quad \text{for} \quad g_0 \gg \gamma \,.$$

If the resonator losses are mainly due to the transmission $T_2$ of the output mirror, the enhancement factor Q then becomes $Q = 1/\gamma = 1/T_2 = q$ which is equal to the enhancement of the previous detection method 1.

Closely above threshold, however, $g_0$ is only slightly larger than $\gamma$ and the denominator in (6.16) becomes very small, which means that the enhancement factor Q may reach very large values (Fig.6.6). At first sight it might appear that the sensitivity could be made arbitrarily large for $2\alpha_0 L \to \gamma$. However, there are experimental as well as fundamental limitations which restrict the maximum achievable value of Q. The increasing instability of the laser output, for instance, limits the detection sensitivity when the threshold is approached. Closely above threshold, the spontaneous radiation which is emitted into the solid angle accepted by the detector cannot be neglected. It represents a constant background intensity, nearly independent



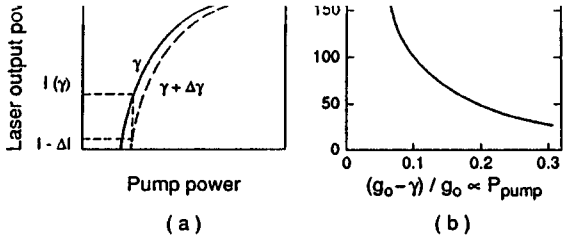


**Fig.6.6.** (a) Laser output power $P_L(P_{pump})$ for two slightly different losses $\gamma$ and $\gamma+\Delta\gamma$. (b) Enhancement factor Q as a function of pump power $P_{pump}$ above threshold

of $\gamma$, which puts a principal upper limit to the relative change $\Delta I/I$ and thus to the sensitivity.

---

**Note**: If the gain medium is inhomogeneously broadened, the saturated gain $g_s$ becomes

$$g_s = \frac{g_0}{\sqrt{1 + I/I_s}}$$

(Sect.3.6 and 7.2). The derivation analogue to (6.13-16) yields instead of (6.16)

$$\frac{\Delta P}{P} = \frac{g_0^2(2\gamma\Delta\gamma + \Delta\gamma^2)}{(g_0^2 - \gamma^2)(\gamma + \Delta\gamma)^2} \simeq \frac{g_0^2}{\gamma^2} \frac{\Delta\gamma}{g_0 - \gamma} \,. \tag{6.18a}$$

---

3) In the preceding discussion of the sensitivity enhancement by intracavity absorption we have implicitly assumed that the laser oscillates in a single mode. Even larger enhancement factors Q can be achieved, however, with lasers oscillating simultaneously in several competing modes. Pulsed or CW dye lasers without additional mode selection are examples of such lasers with mode competition. As discussed in Sect.5.3, the active dye medium exhibits a broad homogeneous spectral gain profile which allows the same dye molecules to simultaneously contribute to the gain of all modes with frequencies within the homogeneous linewidth (see the discussion in Sects. 5.3,8). This means that the different oscillating laser modes may share the same molecules to achieve their gains. This leads to mode competition and exhibits the following mode coupling phenomena:

Assume that the laser oscillates simultaneously on N modes which may have equal gain and equal losses, and therefore equal intensities. When the laser wavelength is tuned across the absorption spectrum of an absorbing sample inside the laser resonator, one of the oscillating modes may be tuned

into resonance with an absorption line (frequency $\omega_k$) of the sample molecules. This mode now suffers additional losses $\Delta\gamma = \alpha(\omega_k)L$ which cause the decrease $\Delta I$ of its intensity. Because of this decreased intensity the inversion of the active medium is less depleted by this mode and the gain at $\omega_k$ *increases*. Since the other (N-1) modes can participate in the gain at $\omega_k$, their intensity will increase. This, however, again depletes the gain at $\omega_k$ and *decreases* the intensity of the mode oscillating at $\omega_k$. With sufficiently strong coupling between the modes this mutual interaction may finally result in a total suppression of the absorbing mode.

Frequency fluctuations of the modes, caused by external perturbations (Sect.5.4) limit the mode coupling. In dye lasers with standing-wave resonators, furthermore, the spatial hole-burning effect (Sect.5.8) weakens the coupling between modes. Because of their slightly different wavelengths the maxima and nodes of the field distributions in the different modes are located at different positions in the active medium. This has the effect that the volumina of the active dye, from which the different modes extract their gain, overlap only partly. With sufficiently high pump power the absorbing mode has an adequate gain volume on its own and is not completely suppressed but suffers a large intensity loss.

A more detailed calculation [6.8,9] yields for the relative power change of the absorbing mode

$$\frac{\Delta P}{P} = \frac{g_0\,\Delta\gamma}{\gamma(g_0 - \gamma)}(1 + KN) \qquad (6.18b)$$

where $K(0 \le K \le 1)$ is a measure of the coupling strength.

Without mode coupling ($K = 0$) (6.18) gives the same result as (6.16) for a single-mode laser. In the case of strong coupling ($K = 1$) and a large number of modes ($N \gg 1$), the relative intensity change of the absorbing mode increases proportional to the number of simultaneously oscillating modes.

If several modes are simultaneously absorbed, the factor N in (6.18) stands for the ratio of all modes to those absorbed. If all modes have equal frequency spacing, their number N gives the ratio of the spectral width of the homogeneous gain profile to the width of the absorption profile.

In order to detect the intensity change of one mode in the prescence of many others, the laser output has to be dispersed by a monochromator or an interferometer. The absorbing molecules may have many absorption lines within the broad-band gain profile of a multimode dye laser. Those laser modes which overlap with absorption lines are attenuated or even completely quenched. This results in "spectral holes" in the output spectrum of the laser and allows the sensitive simultaneous recording of the whole absorption spectrum within the laser bandwidth, if the laser output is photographically recorded behind a spectrograph or if an optical multichannel analyser (Sect.4.5) is used.

4) The discussion in Item 3 has assumed that the mode couplings and mode frequencies were time-independent. In real laser systems this is not true.



Fluctuations of mode frequencies due to density fluctuations of the dye liquid or caused by external perturbations, prevent stationary conditions in a multimode laser. We can define a mean "mode lifetime $t_m$" which represents the average time a specific mode exists in a multimode laser. If the measuring time for intracavity absorption exceeds the mode lifetime $t_m$, no quantitatively reliable information on the magnitude of the absorption coefficient $\alpha(\omega)$ of the intra-cavity sample can be obtained.

It is therefore better to pump the "intracavity laser" with a step-function pump-laser, which starts pumping at $t = 0$ and then stays constant. The intra-cavity absorption is then measured at times t with $0 < t < t_m$, which are shorter than the mean mode lifetime $t_m$. The experimental arrangement is depicted in Fig.6.7 [6.10]. The CW broad-band dye laser is pumped by an argon laser. The pump beam can be switched on by the acousto-optic modulator AOM1 at $t = 0$. The dye-laser output passes a second modulator AOM2 which transmits the dye-laser beam for the time intervall $\Delta t$ at the selectable time t to the entrance slit of a high-resolution spectrograph. A photodiode array with a length D allows simultaneous recording of the spectral intervall $\Delta\lambda = (dx/d\lambda)D$. The repetition rate f of the pump cycles must be smaller than the inverse delay time t between AOM1 and AOM2, i.e. $f < 1/t$.

A detailed consideration [6.8-13] shows that the time evolution of the laser intensity in a specific mode $q(\omega)$ with frequency $\omega$ after the start of the pump pulse depends on the gain profile of the laser medium, the absorption $\alpha(\omega)$ of the intracavity sample and the mean mode lifetime $t_m$. If the broad gain profile with the spectral width $\Delta\omega_g$ and the center frequency $\omega_0$ can be approximated by the parabolic function

$$g(\omega) = g_0\left[1 - \left(\frac{\omega - \omega_0}{\Delta\omega_g}\right)^2\right],$$

the time evolution of the output power $P_q = P(\omega_a)$ in the q-th mode for a constant pumping rate and times $t < t_m$ is after saturation of the gain medium

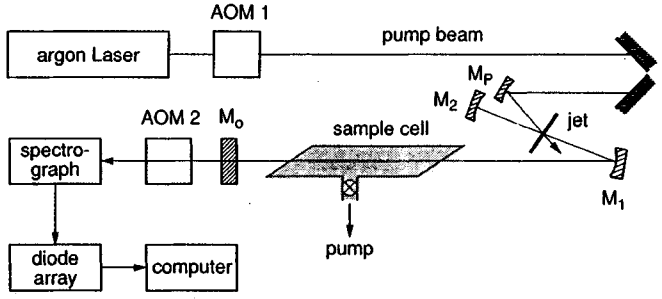


**Fig.6.7.** Experimental arrangement for intracavity laser spectroscopy using a step-function pump intensity and a definite delay for the detection [6.10]

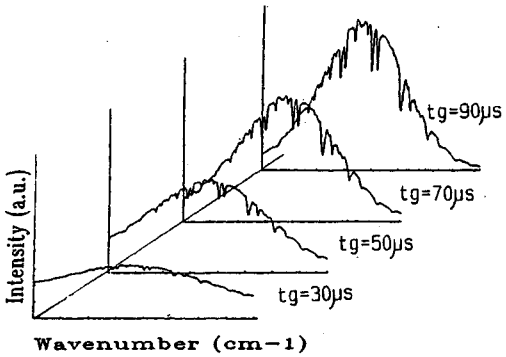


**Fig.6.8.** Time evolution of the spectral profile of the laser output measured with time resolved intracavity absorption spectroscopy [6.10]

$$P_q(t) = P_q(0)\sqrt{\frac{t}{\pi t_m}}\exp\left[-\left(\frac{\omega-\omega_0}{\Delta\omega_g}\right)^2\frac{t}{t_m}\right]e^{-\alpha(\omega_q)ct}\,. \qquad (6.19)$$

The first exponential factor describes the spectral narrowing of the gain profile with increasing time t, and the second factor can be recognized as the Beer-Lambert absorption law with the effective absorption length $L_{eff}$ = ct. The spectral width of the laser output becomes narrower with increasing time but the absorption dips gets more pronounced (Fig.6.8).

---

**Example 6.4**

With typical delay times $t = 10^{-4}$ s the effective absorption pathlength becomes $L_{eff} = 3\cdot10^{8}\cdot10^{-4}$ m = 30 km! If dips of 1% can still be detected, this gives a sensitivity limit of $\alpha \geq 3\cdot10^{-9}$ cm$^{-1}$ for the absorption coefficient $\alpha(\omega)$.

---

In ring lasers (Sect.5.6) the spatial hole-burning effect does not occur if the laser is oscillating in unidirectional travelling-wave modes. If no optical diode is inserted into the ring resonator, the unsaturated gain is generally equal for clockwise and counterclockwise running waves. In such a bistable operational mode slight changes of the net gain which might be different for both waves because of their opposite Doppler shifts, may already switch the laser from clockwise to counterclockwise operation, and vice versa. Such a bistable multimode ring laser with strong gain competition between the modes therefore represents an extremely sensitive detector for small absorptions inside the resonator [6.14].

The enhanced sensitivity of intracavity absorption may be utilized either to detect minute concentrations of absorbing components or to measure very weak forbidden transitions in atoms or molecules at sufficently low pressures to study the unpertubed absorption line profiles. With intracavity absorption cells of less than 1 m, absorbing transitions have been



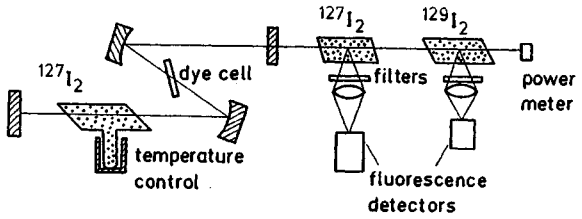


**Fig.6.9.** Isotope selective intracavity absorption spectroscopy. The frequencies $\omega_k$ absorbed by the $^{127}I_2$ isotope inside the laser cavity are missing in the laser output which therefore does not excite any fluorescence in the same isotope outside the laser resonator [6.16]

measured, which would demand a path length of several kilometers with conventional single-pass absorption at a comparable pressure [6.11, 15].

Some examples illustrate the various applications of the intracavity absorption technique.

- With an iodine cell inside the resonator of a CW multimode dye laser an enhancement factor of $Q = 10^5$ could be achieved allowing the detection of $I_2$ molecules at concentrations down to $n \leq 10^8/cm^3$ [6.16]. This corresponds to a sensitivity limit of $\alpha L \leq 10^{-7}$. Instead of the laser output power the laser-induced fluorescence from a second iodine cell outside the laser resonator was monitored as a function of wavelength. This experimental arrangement (Fig.6.9) allows demonstration of the isotope specific absorption. When the laser beam passes through two external iodine cells filled with the isotopes $^{127}I_2$ and $^{129}I_2$ tiny traces of $^{127}I_2$ inside the laser cavity are already sufficient to completely quench the laser-induced fluorescence from the external $^{127}I_2$ cell while the $^{129}I_2$ fluorescence is not affected [6.17]. This demonstrates that those modes of the broad-band dye laser which are absorbed by the internal $^{127}I_2$ are completely suppressed.
- Detection of absorbing transitions with very small oscillator strength (Sect. 2.6.2) has been demonstrated by *Bray* et al. [6.18] who measured with a CW Rhodamine B dye laser (0.3nm bandwidth) the extremely weak ($v'=2$, $v''=0$) infrared overtone absorption band of the red-atmospheric system of molecular oxygen and also the ($v'=6 \leftarrow v''=0$) overtone band of HCl, using a 97-cm long intracavity absorption cell. Sensitivity tests indicated that even transitions with oscillator strenghts down to $f \leq 10^{-12}$ can be readily detected. An example is the P(11) line in the ($2\leftarrow0$) band of the $b^1\Sigma_g^+ \leftarrow x^3\Sigma_g^-$ system of $O_2$ with the oscillator strength $f = 8.4\cdot10^{-13}$ [6.19]!
- The overtone spectrum $\Delta v = 6$ of $SiH_4$ was measured with the effective absorption pathlength $L_{eff}$ = 5.25 km [6.10]. The spectrum shows well-resolved rotational structure and local Fermi resonances were observed.

Although most experiments have so far been performed with dye lasers, the colour-center lasers or the newly developed vibronic solid-state lasers with broad spectral-gain profiles (Sect.5.7.3) are equally well suited for intracavity spectroscopy in the near infrared. An example is the spec-

troscopy of rovibronic transitions between higher electronic states of the $H_3$ molecule with a color-center laser [6.20].

Instead of absorption also weak emission lines can be detected with the intracavity techniques [6.21]. If this light is injected into specific modes of the mulitmode laser, the intensity of these modes will increase for observation times $t < t_m$ before they can share their intensity by mode-coupling with other modes.

A detailed discussion of intracavity absorption, its dynamics and limitations can be found in the articles of *Baev* et al. [6.11,22], in the thesis of *Atmanspacher* [6.19], and in several review articles [6.10,23-27].

## 6.3 Direct Determination of Absorbed Photons

In the methods discussed in the preceding sections the attenuation of the transmitted light (or of the laser power in intracavity spectroscopy) is monitored to determine the absorption coefficient $\alpha(\omega)$ or the number density of absorbing species. For small absorptions this means the measurement of a small difference of two large quantities which limits, of course, the signal-to-noise ratio.

Several different techniques have been developed, where the absorbed radiation power, i.e. the number of absorbed photons can be directly monitored. These techniques belong to the most sensitive detection methods in spectroscopy, and it is worthwhile to know about them.

### 6.3.1 Fluorescence Excitation Spectroscopy

In the visible and ultraviolet regions a very high sensitivity can be achieved, if the absorption of laser photons is monitored through the laser-induced fluorescence (Fig.6.10). When the laser wavelength $\lambda_L$ is tuned to an absorbing molecular transition $E_i \rightarrow E_k$, the number of photons absorbed per second along the path length $\Delta x$ is

$$n_a = N_i n_L \sigma_{ik} \Delta x \tag{6.20}$$

where $n_L$ is the number of incident laser photons per second, $\sigma_{ik}$ the absorption cross section per molecule, and $N_i$ the density of molecules in the absorbing state $|i\rangle$.

The number of fluorescence photons emitted per second from the excited level $E_k$ is

$$n_{fl} = N_k A_k = n_a \eta_k \,, \tag{6.21}$$

where $A_k = \sum_m A_{km}$ stands for the total spontaneous-transition probability (Sect.2.7) to all levels with $E_m < E_k$. The quantum efficiency of the excited



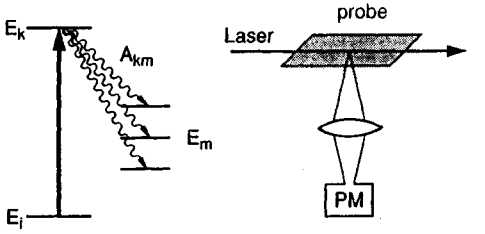


Fig.6.10. Level scheme and experimental arrangement for fluorescence excitation spectroscopy

state, $\eta_k = A_k/(A_k+R_k)$, gives the ratio of the spontaneous transition rate to the total deactivation rate which may also include the radiationless transition rate $R_k$ (e.g., collision-induced transitions). For $\eta_k = 1$ the number $n_{Fl}$ of fluorescence photons emitted per second equals the number $n_a$ of photons absorbed per second under stationary conditions.

Unfortunately only the fraction $\delta$ of the fluorescence photons emitted into all directions, can be collected on the photomultiplier cathode where again only the fraction $\eta_{ph} = n_{pe}/n_{ph}$ of these photons produces on the average $n_{pe}$ photoelectrons. The quantity $\eta_{ph}$ is called the *quantum efficiency of the photocathode* (Sect.4.5.2). The number $n_{pe}$ of photoelectrons counted per second is then

$$n_{pe} = n_a \eta_k \eta_{ph} \delta = (N_i \sigma_{ik} n_L \Delta x) \eta_k \eta_{ph} \delta \,. \tag{6.22}$$

---

**Example 6.5**

Modern photomultipliers reach quantum efficiencies of $\eta_{ph} = 0.2$. With carefully designed optics it is possible to achieve a collection factor $\delta = 0.1$. Using photon counting techniques and cooled multipliers (dark pulse rate $\leq$10 counts/s), counting rates of $n_{pe} = 100$ counts/s are already sufficient to obtain a signal-to-noise ratio S/R ~ 8 at integration times of 1s.

Inserting this figure for $n_{PE}$ into (6.22) illustrates that with $\eta_k = 1$ absorption rates of $n_a = 5 \cdot 10^3$/s can already be measured quantitatively. Assuming a laser power of 1 W at the wavelength $\lambda = 500$ nm which corresponds to a photon flux of $n_L = 3 \cdot 10^{18}$/s, this implies *that it is possible to detect a relative absorption of* $\Delta I/I \leq 10^{-14}$. When placing the absorbing probe inside the cavity where the laser power is q times larger (q ~ 10 to 100, Sect.8.2.3), this impressive sensitivity may be even further enhanced.

---

Since the attainable signal is proportional to the fluorescence collection efficiency $\delta$, it is important to design collection optics with optimum values of $\delta$. Two possible designs are shown in Fig.6.11 which are particularly useful, if the excitation volume is small (e.g., the crossing volume of a laser beam with a collimated molecular beam). One of these collection optics uses a parabolic mirror which collects the light from a solid angle of nearly $2\pi$.

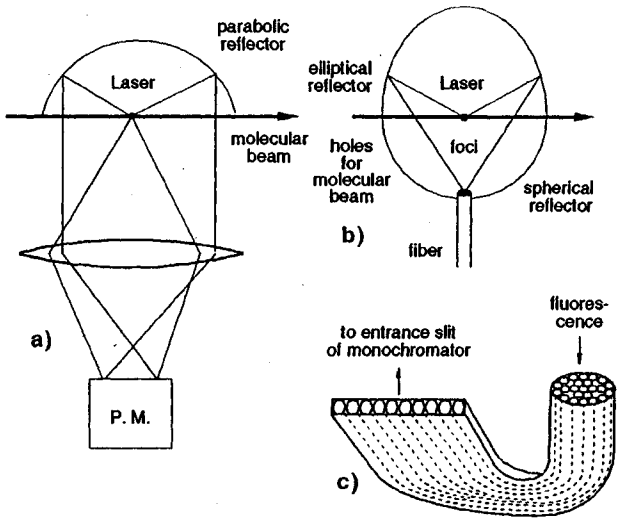


**Fig.6.11.** (a) Parabolic optical system and (b) elliptical/spherical mirror system with high collection efficiency of fluorescence light. (c) Imaging of the fluorescence onto the entrance slit of a monochromator with a properly adjusted shape of the fibre bundle

A lens images the light source onto the photomultiplier cathode. The design of Fig.6.11b uses an elliptical mirror where the light source is placed in one focal point A and the polished end of a multifiber bundle into the other B. A half-sphere reflector with its center in A reflects light, which is emitted into the lower halfspace back into the source A which is then further reflected by the elliptical mirror and focussed into B.

The exit end of the fiber bundle can be arranged to have a rectangular shape in order to match it to the entrance slit of a spectrograph (Fig.6.11c).

When the laser wavelength $\lambda_L$ is tuned across the spectral range of the absorption lines, the total fluorescence intensity $I_{Fl}(\lambda_L) \propto n_L \sigma_{ik} N_i$ monitored as a function of laser wavelength $\lambda_L$, represents an image of the absorption spectrum, called the *excitation spectrum*. According to (6.22) the photoelectron rate $n_{PE}$ is directly proportional to the absorption coefficient $N_i \sigma_{ik}$, where the proportionality factor depends on the quantum efficiency $\eta_{ph}$ of the photo-multiplier cathode and on the collection efficiency $\delta$ of the fluorescence photons.

Although the excitation spectrum directly reflects the absorption spectrum with respect to the line positions, the relative *intensities* of different lines $I(\lambda)$ are identical in both spectra only if the following conditions are guaranteed:

- The quantum efficiency $\eta_k$ must be the same for all excited states $E_k$. Under collision-free conditions, i.e., at sufficiently low pressures, the excited molecules radiate before they can collide, and we obtain $\eta_k = 1$ for all levels $E_k$.



- The quantum efficiency $\eta_{Ph}$ of the detector should be constant over the whole spectral range of the emitted fluorescence. Otherwise the spectral distribution of the fluorescence, which may be different for different excited levels $E_k$, will influence the signal rate. Some modern photomultipliers can meet this requirement.
- The geometrical collection efficiency $\delta$ of the detection system should be identical for the fluroescence from different excited levels. This demand excludes, for examples, excited levels with very long lifetimes, where the excited molecules may diffuse out of the observation region before they emit the fluorscence photon. Furthermore, the fluorescence may not be isotropic, depending on the symmetry of the excited state. In this case $\delta$ will vary for different upper levels.

However, even if these requirements are not strictly fulfilled, excitation spectroscopy is still very useful, to measure absorption lines with extremely high sensitivity, although their relative intensities may not be recorded accurately.

The technique of excitation spectroscopy has been widely used to measure very small absorptions. One example is the determination of absorption lines in molecular beams where both the pathlength $\Delta x$ and the density $N_i$ of absorbing molecules are small.

---

**Example 6.6**

With $\Delta x = 0.1$ cm, $\delta = 0.5$, $\eta = 1$ a density $N_i = 10^7/cm^3$ of absorbing molecules yields for an absorption cross section $\sigma_{ik} = 10^{-17}$ cm$^2$ and an incident flux of $n_L = 10^{16}$ photons/s ($\hat{=}$ 3mW at $\lambda = 500$nm) about $5 \cdot 10^4$ fluorescence photons imaged onto the photomultiplier cathode which emits about $1 \cdot 10^4$ photoelectrons per second.

---

The LIF method is illustrated by Fig.6.12, which shows a section of the excitation spectrum of $Ag_2$, taken in a collimated molecular beam under conditions comparable to that of Example 6.6.

The extremely high sensitivity of this technique has been demonstrated impressively by *Fairbanks* et al. [6.28] who performed absolute density measurements of sodium vapor in the density range $N = 10^2$-$10^{11}$ cm$^{-3}$ using laser-excited fluorescence as monitor. The lower detection limit of $N = 10^2$ cm$^{-3}$ was imposed by background stray light scattered out of the incident laser beam by windows and cell walls.

Because of its high sensitivity, excitation spectroscopy can be successfully used to monitor minute concentrations of radicals and short-lived intermediate products in chemical reactions [6.30]. Besides measurements of small concentrations, detailed information on the internal-state distribution $N_i(v_i'', J_i'')$ of reaction products can be extracted, since the fluorescence signal is, according to (6.22), proportional to the number $N_i$ of absorbing molecules in the level $|i\rangle$ (Sect.6.8.4).

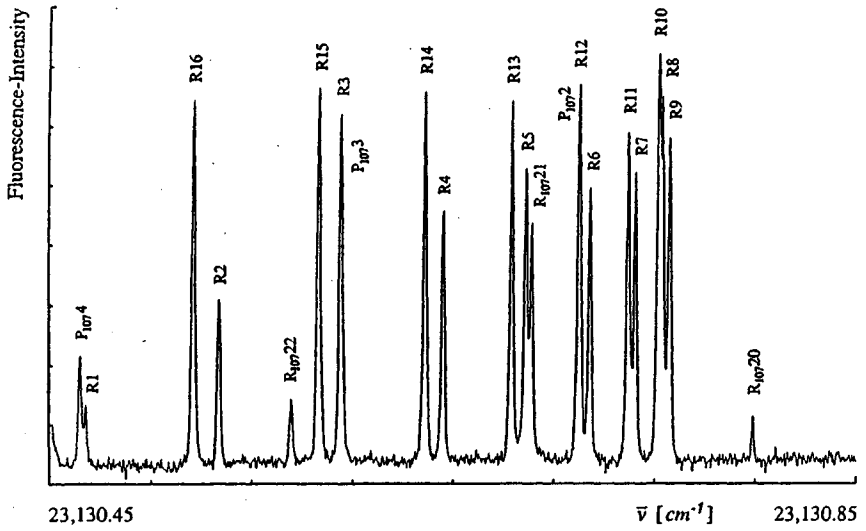


Fig.6.12. Section of the fluorescence excitation spectrum of the $^{107}Ag^{109}Ag$ isotope, showing the band head of the $v' = 1 \leftarrow v'' = 0$ band in the $A^1\Sigma_u \leftarrow X^1\Sigma_g$ system, superimposed by some lines of the $^{107}Ag^{107}Ag$ isotope [6.29]

If in atoms a transition $|i\rangle \rightarrow |k\rangle$ can be selected which represents a true two level system (i.e., the fluorescence from $|k\rangle$ terminates only in $|i\rangle$), the atom may be excited many times while it flies through the laser beam. At a spontaneous lifetime $\tau$ and a travel time T a maximum of $n = T/(2\tau)$ excitation-fluorescence cycles can be achieved (photon burst). With $T = 10^{-5}$ s and $\tau = 10^{-8}$ s we can expect $n = 500$ fluorescence photons per atom!

Excitation spectroscopy has its highest sensitivity in the visible, ultraviolet, and near-infrared regions. With increasing wavelength $\lambda$ the sensitivity decreases for the following reasons: Equation (6.22) shows that the detected photoelectron rate $n_{PE}$ decreases with $\eta_k$, $\eta_{ph}$, and $\delta$. All these numbers generally decrease with increasing wavelength. The quantum efficiency $\eta_{ph}$ and the attainable signal-to-noise ratio are much lower for infrared than for visible photodetectors (Sect.4.5). By absorption of infrared photons vibrational-rotational levels of the electronic ground state are excited with radiative lifetimes which are generally several orders of magnitude larger than those of excited *electronic* states. At sufficiently low pressures the molecules diffuse out of the observation region before they radiate. This diminishes the collection efficiency $\delta$. At higher pressures the quantum efficiency $\eta_k$ of the excited level $E_k$ is decreased because collisional deactivation competes with radiative transitions. Under these conditions photoacoustic detection may become preferable.



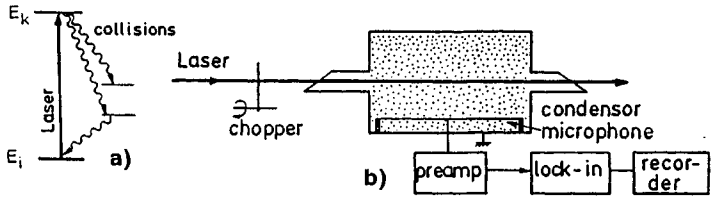


Fig.6.13. Photoacoustic spectroscopy (a) level scheme (b) schematic experimental arrangement

### 6.3.2 Photoacoustic Spectroscopy

This sensitive technique for measuring small absorptions is mainly applied when minute concentrations of molecular species have to be detected in the presence of other components at higher pressure. An example is the detection of spurious pollutant gases in the atmosphere. Its basic principle may be summarized as follows:

The laser beam is sent through the absorber cell (Fig.6.13). If the laser is tuned to the absorbing molecular transition $E_i \rightarrow E_k$, part of the molecules in the lower level $E_i$ will be excited into the upper level $E_k$. By collisions with other atoms or molecules in the cell these excited molecules may tansfer their excitation energy $(E_k - E_i)$ completely or partly into translational, rotational, or vibrational energy of the collision partners. At thermal equilibrium, this energy is randomly distributed onto all degrees of freedom, causing an increase of thermal energy and with it a rise of temperature and pressure at a constant density in the cell.

When the laser beam is chopped at frequencies below 20 kHz, periodical pressure variations appear in the absorption cell which can be detected with a sensitive microphone placed inside the cell. The output signal S [Volt] of the microphone is proportional to the pressure change $\Delta p$ induced by the absorbed radiation power $\Delta W$. If saturation can be neglected, the absorbed energy per cycle

$$\Delta W = N_i \sigma_{ik} \Delta x (1 - \eta_K) P_L \Delta t \qquad (6.23)$$

is proportional to the density $N_i$ [$cm^{-3}$] of the absorbing molecules in level $|i\rangle$, the absorption cross section $\sigma_{ik}$ [$cm^2$], the absorption pathlength $\Delta x$, the cycle period $\Delta t$, and the incident laser power $P_L$. The signal decreases with increasing quantum efficiency $\eta_k$ (which gives the ratio of emitted fluorescence energy to absorbed laser energy) unless the fluorescence is absorbed inside the cell and contributes to the temperature rise.

Since the absorbed energy $\Delta W$ is transferred into kinetic or internal energy of all N molecules per $cm^3$ in the photoacoustic cell with the volume V, the temperature rise $\Delta T$ is obtained from

$$\Delta W = \tfrac{1}{2} f V N k \Delta T \qquad (6.24)$$

ce-Intensity

of degrees of freedom, that are accessible for each of
temperature T [K]. If the chopping frequency of the
gh, the heat transfer to the walls of the cell during the
be neglected. From the equation of state pV = NVkT

$$\frac{2\Delta W}{fV}. \tag{6.25}$$

The output signal from the microphone is then

$$S = \Delta p S_m = \frac{2N_i \sigma_{ik}}{fV} \Delta x (1 - \eta_k) P_L \Delta t S_m \tag{6.26}$$

where the sensitivity $S_m$ [Volt/Pascal] of the microphone not only depends on the characteristics of the microphone but also on the geometry of the photoacoustic cell.

With infrared lasers the molecules are generally excited into higher vibrational levels of the electronic ground state. Assuming cross sections of $10^{-18}$-$10^{-19}$ cm$^2$ for the collisional deactivation of the vibrationally excited molecules, the equipartition of energy takes only about $10^{-5}$ s at pressures around 1 Torr. Since the spontaneous lifetimes of these excited vibrational levels are typically around $10^{-2}$-$10^{-5}$ s, it follows that at pressures above 1 Torr the excitation energy, absorbed from the laser beam, will be almost completely transferred into thermal energy, which implies that $\eta_k \sim 0$.

The idea of the spectraphone is very old and was already demonstrated by Bell and Tyndal [6.31] in 1881. However, the impressive detection sensitivity obtained nowadays could only be achieved with the development of lasers, sensitive capacitance microphones, low-noise amplifiers, and lock-in techniques. Concentrations down to the ppb range (parts per billion = $10^{-9}$) at total pressures of 1 Torr to several atmospheres are readily detectable with a modern spectraphone (Fig.6.14).

Modern condensor microphones with a low-noise FET preamplifier and phase-sensitive detection achieve signals of larger than 1 V/Torr ($\hat{=}$7mV/Pascal) with a background noise of $3 \cdot 10^{-8}$ V at integration times of

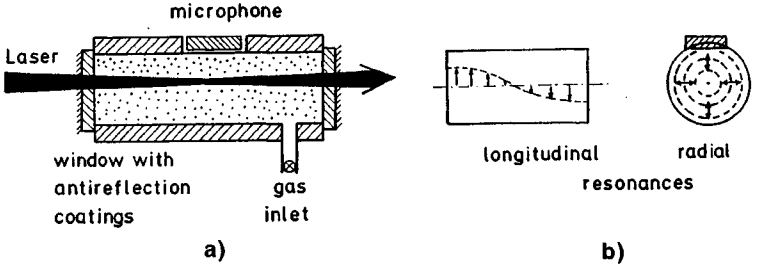


Fig.6.14. (a) Spectraphone with capacitance microphone (b) longitudinal and radial acoustic resonance modes



1 s. This sensitivity allows detection of pressure amplitudes below $10^{-7}$ Torr, and is, in general, not limited by the electronic noise but by another disturbing effect: Laser light reflected from the cell windows or scattered by aerosols in the cell may partly be absorbed by the walls and contributes to a temperature increase. The resulting pressure rise is, of course, modulated at the chopping frequency and is therefore detected as background signal. There are several ways to reduce this phenomenon. Antireflection coatings of the cell windows or, in case of linearly polarized laser light, the use of Brewster windows minimize the reflections. An elegant solution chooses the chopping frequency to coincide with an acoustic resonance of the cell. This results in a resonant amplification of the pressure amplitude which may be as large as 1000-fold. This experimental trick has the additional advantage that those acoustic resonances can be selected, which couple most efficiently to the beam profile but are less effectively excited by heat conduction from the walls. The background signal caused by wall absorption can thus be reduced and the true signal is enhanced. Figure 6.14b shows longitudinal and radial acoustic resonances in a cylindrical cell.

---

**Example 6.7**

With $N_i = 2.5 \cdot 10^{11}$ cm$^{-3}$ ($\hat{=}$ $10^{-8}$ bar), $\sigma_{ik} = 10^{-16}$ cm$^2$, $\Delta x = 10$ cm, $V = 50$ cm$^3$, $\eta_k = 0$, $f = 6$ we obtain the pressure change $\Delta p = 1.5$ Pascal ($\hat{=}$0.01 Torr) for the incident laser power $P_L = 100$ mW. With a microphone sensitivity of $S_m = 10^{-2}$ V/Pascal the output signal becomes $S = 15$ mV.

---

The sensitivity can be further enhanced by frequency modulation of the laser (Sect.6.2.1) and by intracavity absorption techniques. With the spectraphone inside the laser cavity the photoacoustic signal due to nonsaturating transitions is increased by a factor q as a result of a q-fold increase of the laser intensity inside the resonator (Sect.6.2.2).

According to (6.26) the optoacoustic signal decreases with increasing quantum efficiency because the fluorescence carries energy away without heating the gas, as long as the fluorescence light is not absorbed within the cell. Since the quantum efficiency is determined by the ratio of spontaneous to collision-induced deactivation of the excited level, it decreases with increasing spontaneous lifetime and gas pressure. Therefore, the optoacoustic method is particularly favorable to monitor vibrational spectra of molecules in the infrared region (because of the long lifetimes of excited vibrational levels) and to detect small concentrations of molecules in the presence of other gases at higher pressures (because of the large collisional deactivation rate). It is even possible to use this technique for measuring *rotational* spectra in the microwave region and also electronic molecular spectra in the visible or ultraviolet range where electronic states with short spontaneous lifetimes are excited. However, the sensitivity in these spectral regions is not quite as high and there are other methods which are superior.

Some examples illustrate this very useful spectroscopic technique. For a more detailed discussion of optoacoustic spectroscopy, its experimental tricks, and its various applications, the reader is referred to recently published monographs [6.32-34], to some reviews on this field [6.35-38] and to conference proceedings [6.39-41].

---

**Example 6.8**

a) The sensitivity of the spectraphone has been demonstrated by *Kreutzer* et al. [6.42]. At a total air pressure of 500 Torr in the absorption cell these researchers could detect concentrations of ethylene down to 0.2 ppb, of $NH_3$ down to 0.4 ppb, and NO pollutants down to 10 ppb. The feasibility of determining certain important isotope abundances or ratios by simple and rapid infrared spectroscopy with the spectraphone and also the ready control of small leaks of polluting or poison gases has been demonstrated [6.43].

b) The optoacoustic method has been applied with great success to high-resolution spectroscopy of rotational-vibrational bands of numerous molecules [6.44]. Figure 6.15 illustrates as an example a section of the visible overtone absorption spectrum of the $C_2H_2$ molecule where in spite of the small absorption coefficient a good signal-to-noise ratio could be achieved [6.45].

c) A general technique for the optoacoustic spectroscopy of *excited* molecular vibrational states has been demonstrated by *Patel* [6.46]. This technique involves the use of vibrational energy transfer between two dissimilar molecules A and B. When A is excited to its first vibrational level by absorption of a laser photon $h\nu_1$ it can transfer its excitation energy by a near-resonant collision to molecule B. Because of the large cross section for such collisions, a high density of vibrationally excited molecules B can be achieved also for those molecules which cannot be pumped directly by existing powerful laser lines. The excited molecule B can absorb a photon $h\nu_2$ from a second, weak tunable laser, which allows spectroscopy of all accessible transitions ($v=1 \rightarrow v=2$). The technique has been proved for the NO molecule where the frequency of the four transitions in the $^2\Pi_{1/2}$ and $^2\Pi_{3/2}$ subbands of $^{15}NO$ and the $\Lambda$ doubling for the $v=1 \rightarrow 2$ transition have been accurately measured. The following scheme illustrates the method:

$$^{14}NO + h\nu_1(CO_2 \text{ laser}) \rightarrow {}^{14}NO^*(v=1)$$

$$^{14}NO^*(v=1) + {}^{15}NO(v=0) \rightarrow {}^{14}NO(v=0) + {}^{15}NO^*(v=1) + \Delta E(35\,cm^{-1})$$

$$^{15}NO^*(v=1) + h\nu_2(\text{spin-flip laser}) \rightarrow {}^{15}NO^*(v=2)$$

the last process is detected by optoacoustic spectroscopy.

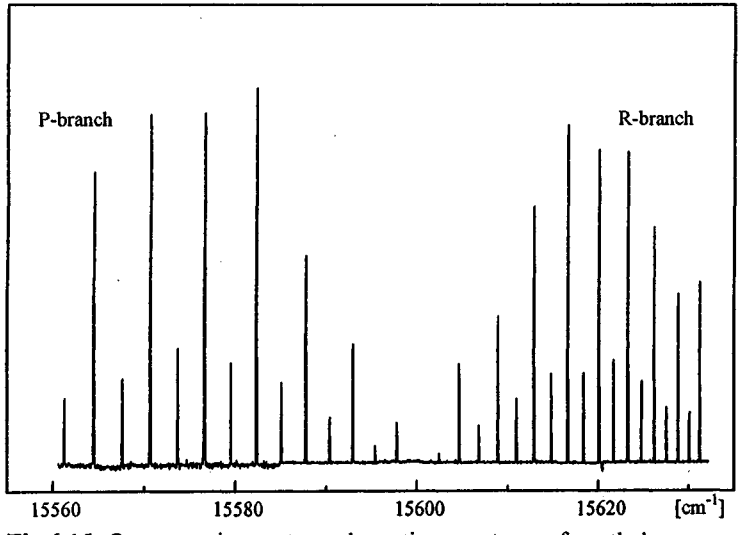


**Fig.6.15.** Optoacoustic overtone absorption spectrum of acethylene around $\bar{\nu} = 15600$ $cm^{-1}$ corresponding to the excitation of a local mode by 5 quanta vibrations [6.45]

d) The application of photoacoustic detection to the visible region has been reported by *Stella* et al. [6.47]. They placed the spectraphone inside the cavity of a CW dye laser and scanned the laser across the absorption bands of the $CH_4$ and $NH_3$ molecules. The high-quality spectra with resolving power of over $2 \cdot 10^5$ proved to be adequate to resolve single rotational features of the very weak vibrational overtone transitions in these molecules. The experimental results prove to be very useful for the investigation of the planetary atmospheres where such weak overtone transitions are induced by the sun light.

e) An interesting application of photoacoustic detection lies in the measurement of dissociation energies of molecules [6.48]. When the laser wavelength is tuned across the dissociation limit, the photoacoustic signal drops drastically because beyond this limit the absorbed laser energy is used for dissociation (which means that it is converted into potential energy and cannot be tansferred into kinetic energy as in the case of excited-state deactivation. Only the kinetic energy causes a pressure increase).

f) With a special design of the spectraphone, employing a coated quartz membrane for the condensor microphone, even corrosive gases can be measured [6.49]. This extends the applications of optoacoustic spectroscopy to aggressive pollutant gases such as $NO_2$ or $SO_2$ which are important constituents of air pollution.

---

The photoacoustic spectroscopy can be also applied to liquids and solids [6.50]. An interesting application is the determination of species absorbed on surfaces. Optoacoustic spectroscopy allows a time-resolved analysis of adsorption- and desorption processes of atoms or molecules at liquid or solid surfaces, and their dependence on the surface characteristics and on the temperature [6.51].

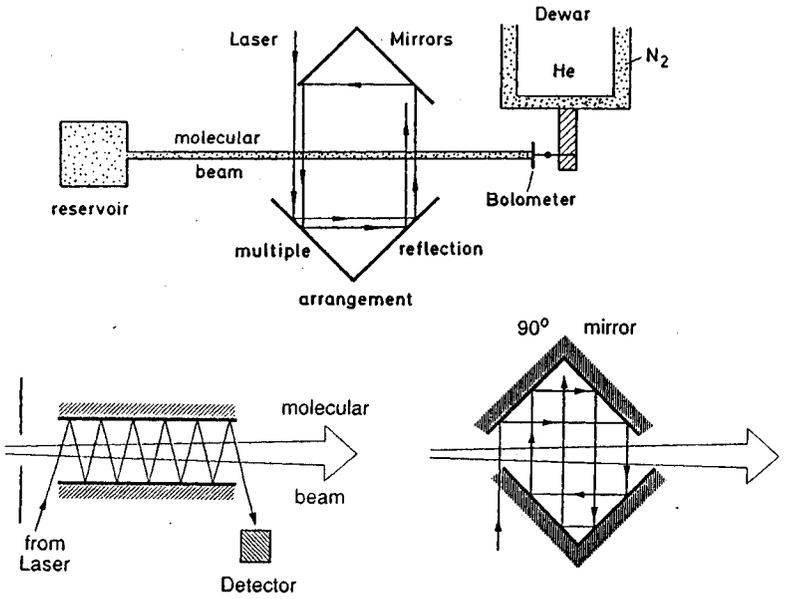


**Fig.6.16.** Optothermal spectroscopy in a molecular beam with a helium-cooled bolometer as detector and two optical systems which increase the absorption path length

### 6.3.3 Optothermal Spectroscopy

For the spectroscopy of vibrational-rotational transitions in molecules the laser-excited fluorescence is generally not the most sensitive tool, as has been discussed at the end of Sect.6.3.1. The optoacoustic spectroscopy, on the other hand, is based on collisional energy transfer and is therefore not applicable to molecular beams, where collisions are rare or even completely absent. For the infrared spectroscopy of molecules in a molecular beam therefore a new detection technique has been developed, which relies on the collision-free conditions in a beam and on the long radiative lifetimes of vibrational-rotational levels in the electronic ground state [6.52].

Optothermal spectroscopy uses a cooled bolometer (Sect.4.5) to detect the excitation of molecules in a beam (Fig.6.16). When the molecules hit the bolometer they transfer their kinetic and their internal thermal energy thereby increasing the bolometer temperature to a stationary value T. If the molecules are excited by a tunable laser (for example, a colour-center laser or a diode laser) their vibrational-rotational energy increases by $\Delta E = h\nu$. If the lifetime $\tau$ of the excited levels is larger than the flight time $t = d/v$ from the excitation region to the bolometer, they transfer this extra energy to the bolometer. If N excited molecules hit the bolometer per second, the rate of heat transfer is

$$\frac{dQ}{dt} = N\Delta E = Nh\nu \,. \tag{6.27}$$



With the heat capacity C of the bolometer and a heat conduction $G(T-T_0)$ the temperature T is determined by

$$Nh\nu = C\frac{dT}{dt} + G(T-T_0) \,. \tag{6.28}$$

Under stationary conditions ($dT/dt = 0$) we obtain from (6.28) the temperature rise

$$\Delta T = T - T_0 = \frac{Nh\nu}{G} \,. \tag{6.29}$$

In general, the exciting laser beam is chopped in order to increase the signal/noise ratio by lock-in detection. The time constant $\tau = C/G$ of the bolometer (Sect.4.5) should be smaller than the chopping period. One therefore has to construct the bolometer in such a way that both C and G are as small as possible.

The temperature change $\Delta T$ can be measured by the resulting resistance change

$$\Delta R = \frac{dR}{dT}\Delta T$$

which is a function of the temperature dependence $dR/dT$ of the bolometer material. Large values of $dR/dT$ are achieved with semiconductor materials at low temperatures (a few Kelvin!). Even larger values can be realized with materials around their critical temperature $T_c$ for the transition from the superconducting to the normal conducting state. In this case, however, one always has to keep the temperature at $T_c$. This can be achieved by a temperature feedback control where the feedback signal is a measure for the rate $dQ/dt$ of energy transfer to the bolometer by the excited molecules.

With such a detector at T = 4 K energy transfer rates $dQ/dt \geq 10^{-12}$ W are still detectable [6.53]. This means that an absorbed laser power of $\Delta P \geq 10^{-12}$ W is measurable. In order to maximize the absorbed power, the absorption path length can be increased by an optical device consisting of two 90° reflectors which reflect the laser beam many times back and forth through the molecular beam (Fig.6.16).

The sensitivity of the optothermal technique is illustrated by the infrared spectrum of a vibrational-rotational transition of the NO molecule with fully resolved hyperfine structure (Fig.6.17). This has been measured with a colour center laser crossed with a collimated NO beam [6.54].

The term "photothermal spectroscopy" is also used in the literature for the generation of thermal-wave phenomena in samples which are illuminated with a time-dependent light intensity [6.55]. In many aspects this is equivalent to photo-acoustic spectroscopy. An interesting modification of this technique for the study of molecules adsorbed at surfaces, is illustrated in Fig.6.18. A small spot of a surface is irradiated by a pulsed-laser beam.

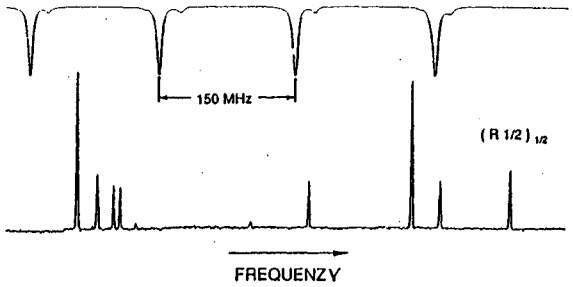


Fig.6.17. Vibration-rotation transition ($v = 0 \rightarrow 2$; $J = 1/2 \rightarrow 3/2$) with resolved hyperfine structure of the NO molecule, measured with optothermal spectroscopy in a collimated molecular beam [6.54]

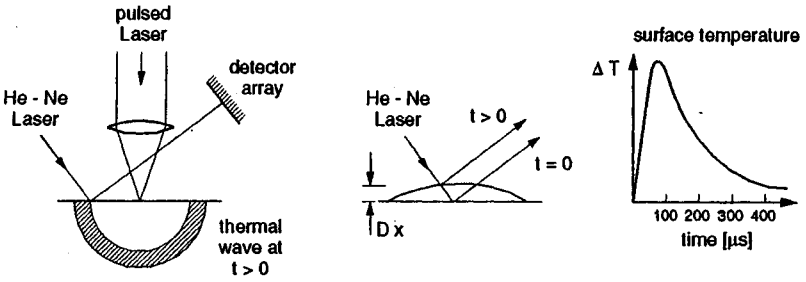


Fig.6.18a-c. Optothermal spectroscopy of solids and of molecules adsorbed at surfaces. (a) Propagation of thermal wave induced by a pulsed laser. (b) Deformation of a surface detected by the deflection of a HeNe laser beam. (c) Time profile of surface temperature change following pulsed illumination [6.56]

The absorbed power results in a temperature rise of the illuminated spot. This temperature will travel as a thermal shock wave through the solid. It leads to a slight time-dependent deformation of the surface, due to thermal expansion. This deformation is probed by the time-dependent deflection of a low-power HeNe laser. In case of adsorbed molecules the absorbed power varies when the laser wavelength is tuned over the absorption spectrum of the molecules. Time-resolved measurements of the probe-beam deflection allows one to determine the kind and amount of adsorbed molecules and to follow up their desorption with time, caused by the irradiating light [6.56].

## 6.4 Ionization Spectroscopy

Ionization spectroscopy monitors the absorption of photons on the molecular transition $E_i \rightarrow E_k$ by detecting the ions or electrons, produced by some means, while the molecule is in its excited state $E_k$.



### 6.4.1 Basic Techniques

The necessary ionization of the excited molecule may be performed by photons, by collisions, or by an external electric field:

#### a) Photoionization

The excited molecules can be ionized by absorption of a second photon, i.e.,

$$M^*(E_k) + h\nu_2 \rightarrow M^+ + e^- + E_{kin} \,. \tag{6.30a}$$

The ionizing photon may come either from the same laser which has excited the level $E_k$ or from a separate light source, which can be another laser or even an incoherent source (Fig.6.19a).

A very efficient photionization process is the excitation of high-lying Rydberg levels above the ionization limit (Fig.6.19b) which decay by autoionization into lower levels of the ion $M^+$

$$M^*(E_k) + h\nu_2 \rightarrow M^{**} \rightarrow M^+ + e^- + E_{kin} \,. \tag{6.30b}$$

The absorption cross-section for this process is generally much larger than that of the "bound-free transition" described by (6.30a) (Sect.10.4.2).

The excited molecule may also be ionized by a nonresonant two-photon process (Fig.6.19c)

$$M^*(E_k) + 2h\nu_2 \rightarrow M^+ + e^- + E_{kin} \,. \tag{6.30c}$$

#### b) Collision-Induced Ionization

Ionizing collisions between excited atoms or molecules and electrons represent the main ionization process in gas discharges.

$$M^*(E_k) + e^- \rightarrow M^+ + 2e^- \,. \tag{6.31a}$$

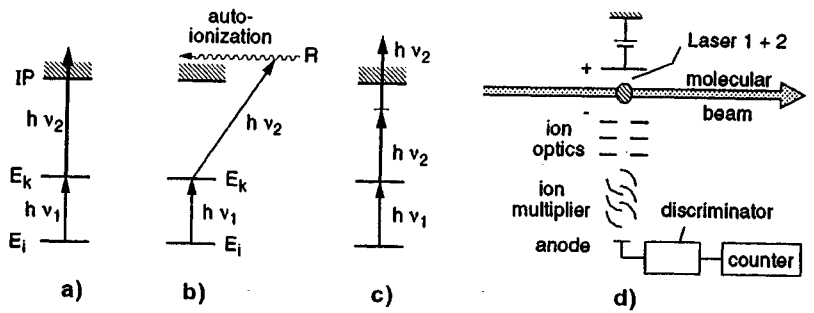


Fig.6.19a-d. Level schemes of ionization spectroscopy. (a) Photo-ionization, (b) excitation of auto-ionizing Rydberg levels, (c) two-photon ionization of excited molecules, (d) experimental arrangement for photoionization spectroscopy in a molecular beam

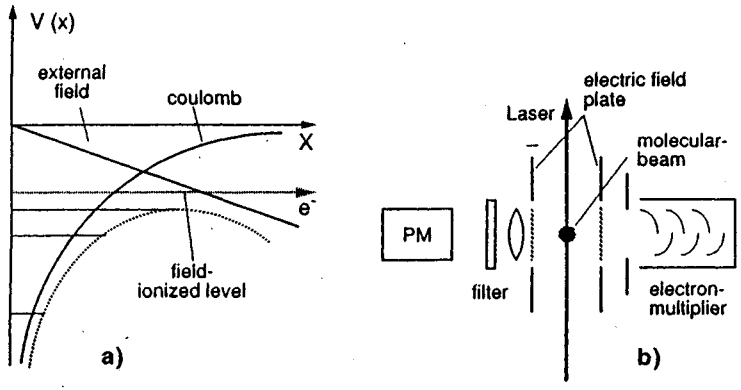


**Fig.6.20a,b.** Field ionization of highly excited levels closely below the ionization limit: (a) Potential diagram and (b) experimental arrangement for field ionization in a molecular beam. The photomultiplier monitors the LIF from the intermediate level populated in a two-step excitation process

If the excited level $E_k$ is not too far from the ionization limit, the molecule may also be ionized by thermal collisions with other atoms or molecules. If $E_k$ lies above the ionization limit of the collision partners A, Penning ionization [6.57] becomes an efficient process which proceeds as

$$M^*(E_k) + A \rightarrow M + A^+ + e^- \quad . \tag{6.31b}$$

### c) Field Ionization

If the excited level $E_k$ lies closely below the ionization limit, the molecule $M^*(E_k)$ can be ionized by an external electric DC field (Fig.6.20a). This method is particularly efficient if the excited level is a long-lived highly excited Rydberg state. The required minimum electric field can readily be estimated from Bohr's atomic model, which gives a good approximation for atomic levels with large principal quantum number n. The ionization potential for the outer electron at the mean radius r from the nucleus is determined by the Coulomb field of the nucleus shielded by the inner electron core.

$$IP = \int_r^\infty \frac{Z_{eff}e^2}{4\pi\epsilon_0 r^2}dr = \frac{Z_{eff}e^2}{4\pi\epsilon_0 r}$$

where $eZ_{eff}$ is the effective nuclear charge, i.e. the nuclear charge eZ partly screened by the electron cloud. If an external field $E_{ext} = -E_0 x$ is applied, the effective ionization potential is lowered to the value

$$IP_{eff} = IP - \sqrt{\frac{Z_{eff}e^3 E_0}{\pi\epsilon_0}} \quad . \tag{6.32}$$



If the energy E of the excited level is above $IP_{eff}$, it will be field-ionized.

Techniques, where the laser excites the atoms, but the ionizing step is performed by field ionization, have found increasing applications in the detection of Rydberg atoms in molecular beams (Sect.14.6), in analytical chemistry for trace elements or small concentrations of pollutants [6.58].

---

**Example 6.9**

For levels 10 meV below the ionization limit, (6.32) gives $E_0 \geq 1.7 \cdot 10^4$ V/m for the ionizing external field. However, because of the quantum-mechanical tunnel effect the fields required for complete ionization are even lower.

---

## 6.4.2 Sensitivity of Ionization Spectroscopy

The following estimation illustrates the possible sensitivity of ionization spectroscopy (Fig.6.19a). Let $N_k$ be the density of excited molecules in level $E_k$, $P_{kI}$ the probability per second that a molecule in level $E_k$ is ionized, and $n_a$ the number of photons absorbed per second on the transition $E_i \rightarrow E_k$. If $R_k$ is the total relaxation rate of level $E_k$, besides the ionization rate (spontaneous transitions plus collision-induced deactivation) the signal rate in counts per second is for the absorption path length $\Delta x$ and for $n_L$ incident laser photons per second:

$$S_I = N_k P_{kI} \delta \cdot \eta = n_a \frac{P_{kI}}{P_{kI} + R_k} \delta \cdot \eta = N_i n_L \sigma_{ik} \Delta x \frac{P_{kI}}{P_{kI} + R_k} \delta \cdot \eta \quad . \tag{6.33}$$

With a proper design the *collection* efficiency $\delta$ for the ionized electrons or ions can reach $\delta = 1$. If the electrons or ions are accelerated to several keV and detected by electron multipliers or channeltrons a *detection* efficiency of $\eta = 1$ can be achieved, too. If the ionization probability $P_{kI}$ can be made large compared to the relaxation rate $R_k$ of the level $|k\rangle$ the signal $S_I$ then becomes with $\delta = \eta = 1$:

$$S_I \sim n_a \quad .$$

This means that every laser photon absorbed in the transition $E_i \rightarrow E_k$ gives rise to a detected ion or electron. It implies that *single absorbed photons* can be detected with an overall efficiency close to unity (or 100%). In experimental practice there are, of course, additional losses and sources of noise, which limit the detection efficiency to a somewhat lower level. However, for all absorbing transitions $E_i \rightarrow E_k$, where the upper level $E_k$ can readily be ionized, ionization spectroscopy is the most sensitive detection technique and superior to all other methods discussed so far [6.59,60].

### 6.4.3 Pulsed vs CW Lasers for Photoionization

In case of photoionization of the excited level $|k\rangle$ the ionization probability per second

$$P_{kI} = \sigma_{kI} n_{L_2} \quad [s^{-1}]$$

equals the product of the ionization cross section $\sigma_{kI}$ [$cm^2$] and the photon flux density $n_{L_2}$ [$cm^{-2} \cdot s^{-1}$] of the ionizing laser. We can then write (6.33) as

$$S_I = N_i \left[ \frac{\sigma_{ik} n_{L_1} \delta \cdot \eta}{1 + R_k/(\sigma_{kI} n_{L_2})} \right] \Delta x \,. \tag{6.34}$$

The maximum ion rate $S_I^{max}$ which is achieved if

$$\sigma_{kI} n_{L2} >> R_k$$

becomes equal to the rate $n_a$ of photons absorbed in the transition $|i\rangle \rightarrow |k\rangle$:

$$S_I^{max} = N_i \sigma_{ik} n_{L_1} \Delta x = n_a \,. \tag{6.35}$$

The following estimation illustrates whether this maximum ion rate can be realized: Typical cross sections for photoionization are $\sigma_{kI} \sim 10^{-17}$ $cm^2$. If radiative decay is the only deactivation mechanism of the excited level $|k\rangle$ we have $R_k = A_k \approx 10^8$ $s^{-1}$. In order to achieve $n_{L_2} \sigma_{kI} > A_k$ we need a photon flux $n_{L_2} > 10^{25}$ $cm^{-2} \cdot s^{-1}$ of the ionizing laser. With pulsed lasers this condition can be met readily.

---

**Example 6.10**

Excimer laser: 100 mJ/pulse, $\Delta T = 10$ ns, the cross section of the laser beam may be 1 $cm^2 \rightarrow n_{L2} = 2 \cdot 10^{25}$ $cm^{-2} \cdot s^{-1}$. With the numbers above we can reach an ionization probability of $P_{ik} = 2 \cdot 10^8$ $s^{-1}$ for all molecules within the laser beam. This gives an ion rate $S_I$ which is 2/3 of the maximum rate $S_I = n_a$.

---

The advantage of pulsed lasers is the large photon flux during the pulse time $\Delta T$ which allows the ionization of the excited molecules *before they decay* by relaxation into lower levels where they are lost for further ionization. Their disadvantages are their large spectral bandwidth that is generally larger than the Fourier-limited bandwidth $\Delta\nu \geq 1/\Delta T$ and their low duty cycle. At typical repetition rates of $f_L = 10$ to 100 $s^{-1}$ and a pulse duration of $\Delta T = 10^{-8}$ s the duty cycle is only $10^{-7}$ - $10^{-6}$!



If the diffusion time $t_D$ of molecules out of the excitation-ionization region is smaller than $1/f_L$, at most the fraction $f_L t_D$ of molecules can be ionized, even if the ionization probability during the laser pulse $\Delta T$ approaches 100%.

---

**Example 6.11**

Assume that the two laser beams L1 and L2 for excitation and ionization have the diameter D = 1 cm and traverse a collimated molecular beam with 1 $cm^2$ cross section perpendicularly. During the pulse time $\Delta T = 10^{-8}$ s the distance, travelled by the molecules at the mean velocity $\bar{v} = 500$ m/s is $d = \Delta T \bar{v} \sim 5 \cdot 10^{-4}$ cm. This means that all molecules in the excitation volume of 1 $cm^3$ can be ionized during the time $\Delta T$. During the "dark" time $T = 1/f_L$, however, the molecules travel the distance $d = \bar{v}T \sim 500$ cm at $f_L = 10^2$ $s^{-1}$. Therefore, only the fraction $1/500 = 2 \cdot 10^{-3}$ of all molecules in the absorbing level $|i\rangle$ are ionized in a continuous molecular beam.

There are two solutions:

(i) If pulsed molecular beams can be employed having the pulse time $\Delta T_B \leq D/\bar{v}$ and the repetition rate $f_B = f_L$, an optimum detection probability can be achieved.

(ii) In continuous molecular beams the two laser beams may propagate antiparallel to the molecular-beam axis. If lasers with a high-repetition frequency $f_L$ are used (for example, copper-laser-pumped dye lasers with $f_L \leq 10^4 s^{-1}$), then the distance travelled by the molecules during the dark time is only $d = \bar{v}/f \geq 5$ cm. They can therefore still be detected by the next pulse [6.61,62].

---

With CW lasers the duty cycle is 100% and the spectral resolution is not limited by the laser bandwidth. However, the laser beam has to be focussed in order to meet the requirement $P_{kI} > R_k$.

---

**Example 6.12**

If a CW argon laser with 10 W at $\lambda = 488$ nm ($\hat{=} 2.5 \cdot 10^{19}$ photon/s) is used for the ionizing step, it has to be focussed down to an area of $1.5 \cdot 10^{-6}$ $cm^2$, i.e. a diameter of 10 $\mu$m in order to reach a photon flux density of $n_{L2} = 10^{25}$ $cm^{-2} \cdot s^{-1}$.

---

Here the following problem arises: The molecules excited by laser L1 into level $|k\rangle$ travel during their spontaneous lifetime of $\tau = 10$ ns at the thermal velocities $\bar{v} = 5 \cdot 10^4$ m/s only a distance of $d = 5$ $\mu$m before they decay into lower levels. The second laser L2 has therefore to be focussed in a similar way as L1 and its focus has to overlap that of L1 within a few $\mu$m.

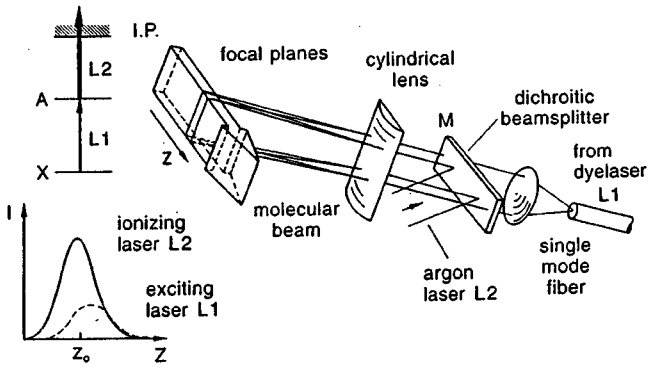


**Fig.6.21.** Experimental arrangement for resonant two-photon two-colour ionization with two CW lasers. The insert shows the optimum overlap of the Gaussian intensity profiles in the focal plane

A technical solution of this problem is depicted in Fig.6.21. The dye laser L1 is guided through a single-mode optical fiber. The divergent light, emitted out of the fiber end is made parallel by a spherical lens, superimposed with the beam of the argon laser L2 by a dichroic mirror M. Both beams are then focussed by a cylindrical lens into the molecular beam, forming there a rectangular "sheet of light" with a thickness of about 5÷10 $\mu$m and a height of about 1 mm, adapted to the dimensions of the molecular beam [6.63]. All molecules in the beam have to pass through the two laser beams. Since the transition probability for the first step $|i\rangle \rightarrow |k\rangle$ is generally larger by some orders of magnitude than that of the ionizing transition, the first transition can be readily saturated (Sect.7.1). It is therefore advantageous, to adjust the relative positions of the two beams in such a way, that the maximum intensity of L2 coincides spatially with the slope of the Gaussian intensity profile of L1 (see insert of Fig.6.21).

Often it is possible to tune the ionizing laser L2 to transitions from $|k\rangle$ into autoionizing Rydberg levels (Sect.10.4). For such transitions the probability may be 2÷3 orders of magnitude larger than for bound-free transitions into the ionization continuum. In these cases the requirement (6.35) can be met already at much lower intensities of L2.

The resonant two-step ionization with two laser photons from pulsed or CW lasers represents the most versatile and sensitive detection technique. If laser L1 excites all atoms or molecules which fly through the laser beam, single atoms or molecules can be detected [6.59,64,65] if the condition (6.35) can be fulfilled.

### 6.4.4 Resonant Two-Photon Ionization Combined with Mass Spectrometry

In combination with mass spectrometry isotope selective spectroscopy becomes possible, even if the spectral lines of the different isotope spectra



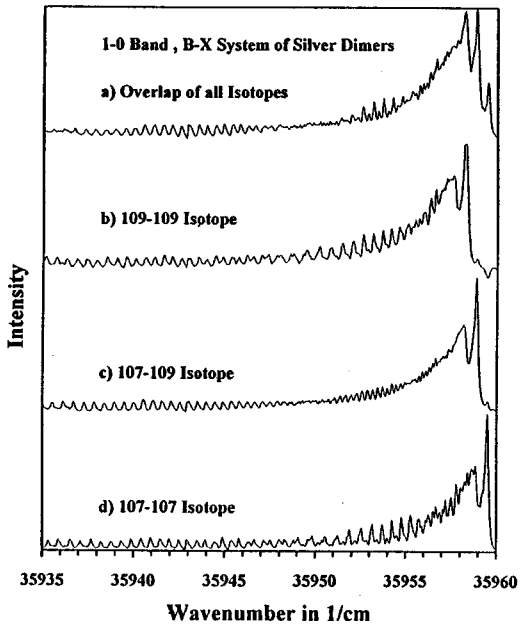


**Fig.6.22.** Photoionization spectrum of the $0 \leftarrow 1$ band in the $B \leftarrow X$ system of $Ag_2$. (*a*) Overlap of the three isotopes $^{107}Ag^{107}Ag$, $^{107}Ag^{109}Ag$ and $^{109}Ag^{109}Ag$, showing 3 band heads. (*b-d*) Separate spectra of the 3 isotopes obtained behind a time of flight spectrometer with three parallel time-gated detectors [6.67]

overlap. This is, in particular, important for *molecular* isotopes with dense spectra, which overlap for the different isotopes (Fig.6.22).

With pulsed lasers time-of-flight mass spectrometers are convenient since they allow the simultaneous but separate recording of the spectra of different isotopes [6.66,67]. For ionization by CW lasers quadrupole mass spectrometers are generally used. Their disadvantage is the lower transmittance and the fact that different masses cannot be recorded simultaneously but only sequentially. At sufficiently low ion rate delayed coincidence techniques in combination with time-of-flight spectrometers can be utilized if both the photoion and the corresponding photoelectron are detected. The detected electron provides the zero point of the time scale and the ions with different masses are separated by their differences $\Delta t_a = t_{ion} - t_{el}$ in arrival times at the ion detector.

For measurements of cluster-size distributions in cold molecular beams (Sect.9.3), or for monitoring the mass distribution of laser-desorbed molecules from surfaces, these combined techniques of laser ionization and mass spectrometry are very useful [6.68,69]. For the detection of rare isotopes in the presence of much more abundant other isotopes the double discrimination of isotope-selective excitation by the first laser L1 and the subsequent mass separation by the mass spectrometer is essential to completely separate the isotopes even if the far wings of their absorption lines overlap [6.70].

The combination of REsonant MultiPhoton Ionization (REMPI) with mass spectrometry for the investigation of molecular dynamics and fragmentation is discussed in Chap.10.

### 6.4.5 Thermionic Diode

The collisional ionization of high-lying Rydberg levels is utilized in the thermionic diode [6.71] which consists of a metallic cylindrical cell filled with a gas or vapor, a heated wire as cathode and the walls as anode (Fig.6.23). If a small voltage of a few volts is applied, the diode operates in the space charge limited region and the diode current is restricted by the electron space charge around the cathode. The laser beam passes through this space charge region close to the cathode and excites molecules into Rydberg states which are ionized by electron impact. Because of its much larger mass the ion stays on the average a much longer time $\Delta t_{ion}$ within the space-charge region than an electron. During this period it compensates one negative charge and therefore allows $n = \Delta t_{ion}/\Delta t_{el}$ extra electrons to leave the space-charge region. If N ions are formed per second the diode current therefore increases by

$$\Delta i = eN\Delta t_{ion}/\Delta t_{el} = eMN\,. \qquad (6.36)$$

The current magnification factor M can reach values of up to $M = 10^5$.

With thermionic diodes sensitive and accurate measurements of atomic and molecular Rydberg levels have been performed [6.72-74]. With a special arrangement of the electrodes a nearly field-free excitation zone can be realized which allows the measurement of Rydberg states up to the principal quantum numbers n = 300 [6.74] without noticeable Stark shifts.

A more detailed representation of ionization spectroscopy and its various applications to sensitive detection of atoms and molecules can be found in [6.58-60, 64-66].

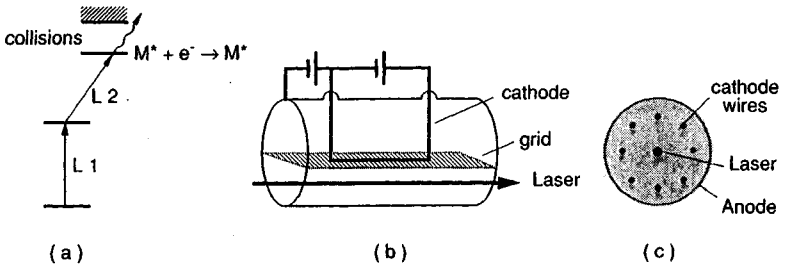


**Fig.6.23a-c.** Thermionic diode. (a) Level scheme, (b) schematic arrangement and (c) field free excitation scheme, where the laser beam passes through the field-free central region in a symmetric arrangement of cathode wires



## 6.5 Optogalvanic Spectroscopy

Optogalvanic spectroscopy is an excellent and simple technique to perform laser spectroscopy in gas discharges. Assume that the laser beam passes through part of the discharge volume. When the laser frequency is tuned to the transition $E_i \rightarrow E_k$ between two levels of atoms or ions in the discharge, the population densities $n_i(E_i)$ and $n_k(E_k)$ are changed by optical pumping. Because of the different ionization probabilities from the two levels, this population change will result in a change $\Delta I$ of the discharge current which is detected as a voltage change $\Delta U = R\,\Delta I$ across the ballast resistor R (Fig.6.24). When the laser intensity is chopped, an AC voltage is obtained which can be directly fed into a lock-in amplifier.

Already with moderate laser powers (a few milliwatts) large signals ($\mu$V to mV) can be achieved in gas discharges of several milliamperes. Since the absorbed laser photons are detectd by the optically induced current change, this very sensitive technique is called *optogalvanic spectroscopy* [6.75-77].

Both positive and negative signals are observed, depending on the levels $E_i$, $E_k$ involved in the laser-induced transition $E_i \rightarrow E_k$. If $IP(E_i)$ is the total ionization probability of an atom in level $E_i$, the voltage change $\Delta U$ produced by the laser-induced change $\Delta n_i = n_{i0} - n_{iL}$ is given by

$$\Delta U = R\,\Delta I = a[\Delta n_i IP(E_i) - \Delta n_k IP(E_k)]\,. \qquad (6.37)$$

There are several competing processes which may contribute to the ionization of atoms in level $E_i$, such as direct ionization by electron impact $A(E_i)+e^- \rightarrow A^+ + 2e$, collisional ionization by metastable atoms $A(E_i)+B^* \rightarrow A^+ + B + e^-$, or, in particular for highly excited levels, the direct photoionization by laser photons $A(E_i)+h\nu \rightarrow A^+ + e^-$. The competition of these and other processes determines whether the population changes $\Delta n_i$ and $\Delta n_k$ cause an increase or a decrease of the discharge current. Figure 6.25a shows the optogalvanic spectrum of a Ne discharge (5mA) recorded in a fast scan

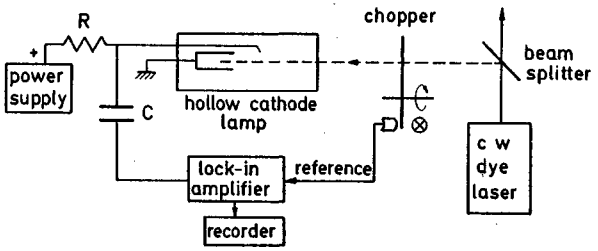


**Fig.6.24.** Experimental arrangement of opto-galvanic spectroscopy in a hollow cathode lamp

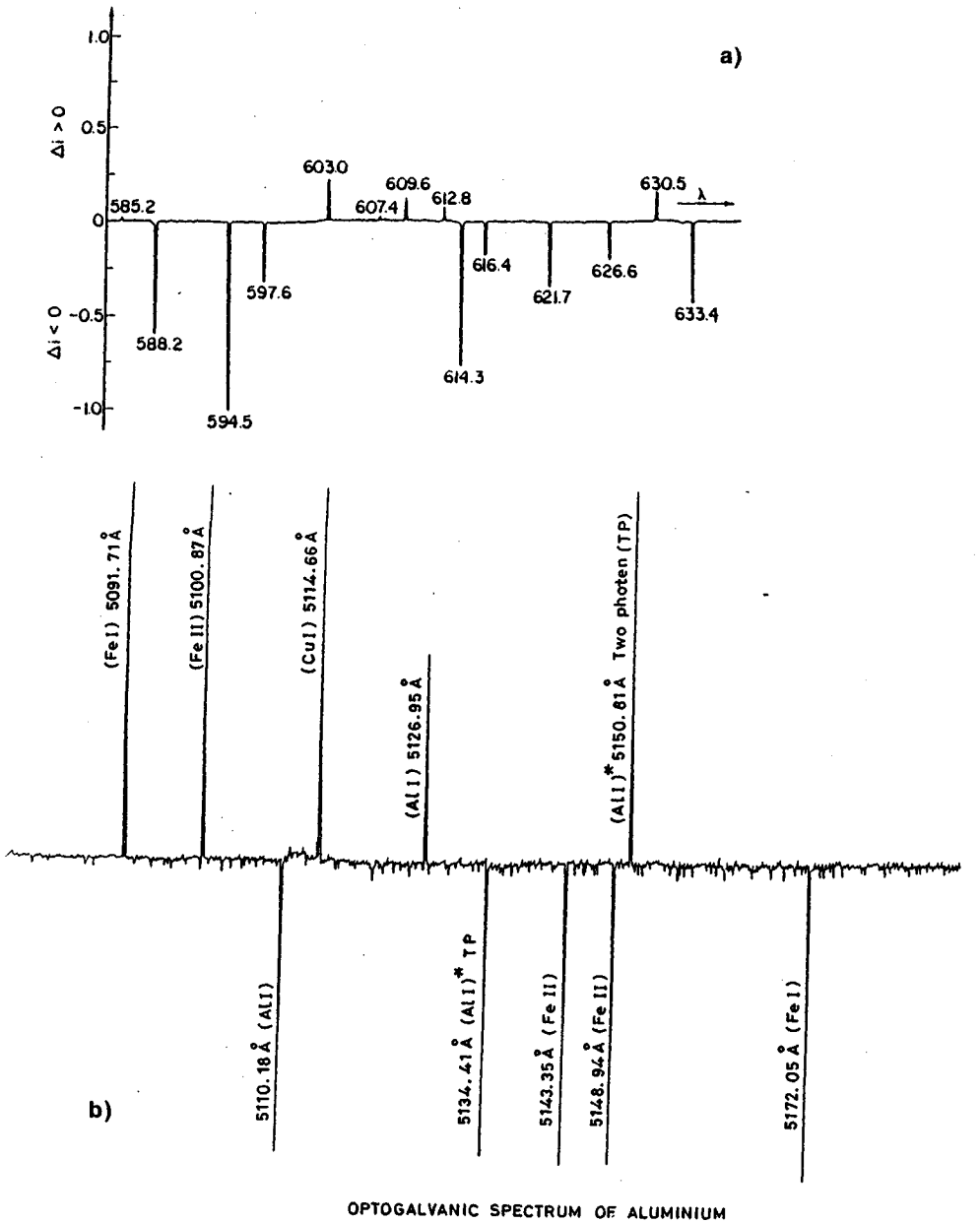


Fig.6.25. Opto-galvanic spectra (**a**) of a neon discharge (1mA, p = 0.8torr), generated with a broad band CW dye laser [6.77] and (**b**) of Al and Fe vapor sputtered in two hollow cathode discharges and simultaneously illuminated with a pulsed dye laser [6.78]

with 0.1 s time constant. The good signal-to-noise ratio demonstrates the sensitivity of the method.

In hollow cathodes the cathode material can be sputtered by ion bombardment in the discharge. The metal vapor, consisting of atoms and ions, can be investigated by optogalvanic spectroscopy. Figure 6.25b illustrates a section of the optogalvanic spectrum of aluminum and iron atoms and ions $Al^+$, $Fe^+$, measured simultanously in two hollow cathodes irradiated with a tunable pulsed dye laser [6.78].

Also molecular spectra can be measured by optogalvanic spectroscopy [6.79]. In particular, transitions from highly excited molecular states that are not accessible to optical excitation, but are populated by electron impact in the gas discharge can be investigated. Furthermore, molecular ions and radicals can be studied. Some molecules, called *excimers* (Sect.5.9) are only stable in their excited states. They are therefore predistinated for this technique because they do not exist in the ground state and cannot be studied in neutral-gas cells. Examples are $He_2^*$ or $H_2^*$ [6.80,81].

Optogalvanic spectroscopy is a suitable technique for studies of excitation and ionization processes in flames, gas discharges and plasmas [6.82]. Of particular interest is the investigation of radicals and unstable reaction products which are formed by electron-impact fragmentation in gas discharges. These species play an important role in the extremely rarefied plasma in molecular clouds in the interstellar medium.

Besides its applications to studies of collision processes and ionization probabilities in gas discharges and combustion processes, this technique has the very useful aspect of simple wavelength calibration in laser spectroscopy [6.83]. A small fraction of the output from a tunable laser is split into a hollow-cathode spectral lamp and the optogalvanic spectrum of the discharge is recorded simultaneously with the unknown spectrum under investigation. The numerous lines of thorium or uranium are nearly equally distributed throughout the visible and ultraviolet spectral regions (Fig.6.26). They are recommended as secondary wavelength standards since they have been measured interferometrically to a high precision [6.84,85]. They can therefore serve as convenient absolute wavelength markers, accurate to about 0.001 $cm^{-1}$.

If the discharge cell has windows of optical quality, it can be placed inside the laser resonator taking advantage of the q-fold laser intensity (Sect.6.2.2). With such an intracavity arrangement Doppler-free saturation spectroscopy can also be performed with the optogalvanic technique (Sect.7.2 and [6.86]). An increased sensitivity can be achieved by optogalvanic spectroscopy in thermonic diodes under space-charge-limited conditions (Sect.6.4.5). Here the internal space charge amplification is utilized to generate signals in the mV to V range without further external amplification [6.72,87].

For more details on optogalvanic spectroscopy see the reviews [6.58, 75-78] and the book [6.88], which also give extensive reference lists.

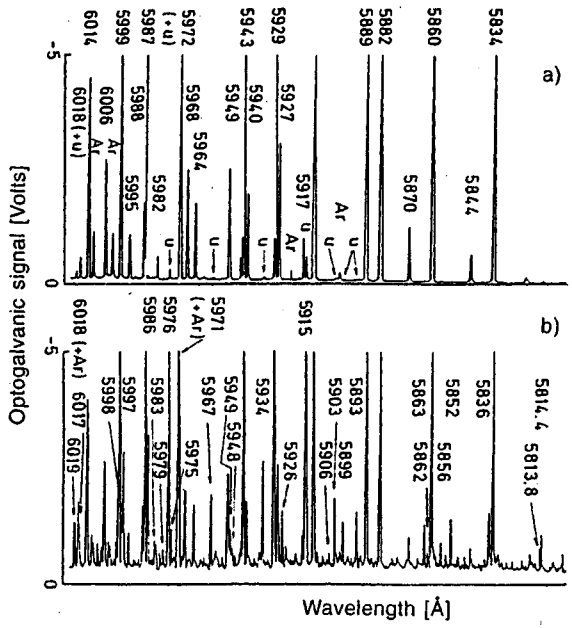


**Fig.6.26a,b.** Optogalvanic spectrum of an Uranium hollow cathode lamp filled with argon as buffer gas. In the upper spectrum (a), taken at 7 mA discharge current, most of the lines are argon transitions while in the lower spectrum (b) at 20 mA many more uranium lines appear, due to sputtering of uranium from the hollow cathode walls [6.83]

## 6.6 Velocity-Modulation Spectroscopy

The analysis of absorption spectra in molecular-gas discharges is by no means simple, because the gas discharge produces from the neutral parent molecules a large variety of neutral and ionized fragments. The spectra of these different species may overlap and often an unambiguous identification is not possible if the spectra are not known. An elegant technique, developed by *Saykally* et al. [6.89,90] is very helpful in distinguishing between spectra of ionized and neutral species.

The external voltage applied to the gas discharge accelerates the positive ions towards the cathode and the negative ions towards the anode. They acquire therefore a drift velocity $v_D$ which causes a corresponding Doppler shift $\Delta\omega = \omega - \omega_0 = \mathbf{k}\cdot\mathbf{v}_D$ of their absorption frequency $\omega_0$. If an AC voltage of frequency f is applied instead of a DC voltage, the drift velocity is periodically changed and the absorption frequency $\omega = \omega_0 + \mathbf{k}\cdot\mathbf{v}_D$ is modulated at the frequency f around the unshifted frequency $\omega_0$. When the absorption spectrum is recorded with a lock-in amplifier, the spectra of the ions can be immediately distinguished from those of the neutral species. This velocity modulation technique has the same effect as the frequency modulation discussed in Sect.6.2.1. When the laser is scanned through the spectrum, the first derivatives of the ion lines are seen where the phase of the signals is opposite for positive and negative ions, respectively (Fig.6.27). The two species can therefore be distinguished by the sign of the lock-in output signal.

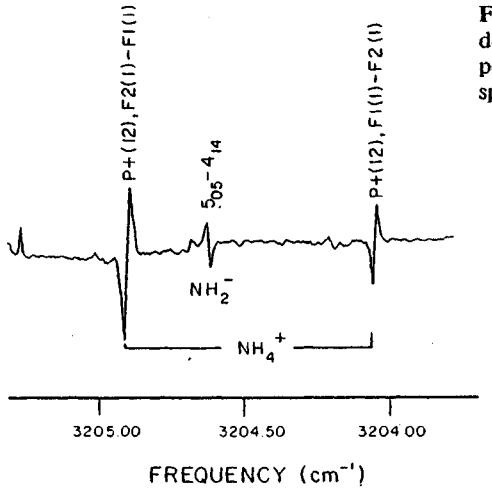


**Fig.6.27.** Opposite signal phases of the derivative line profiles of negative and positive ions in velocity modulation spectroscopy [6.89]

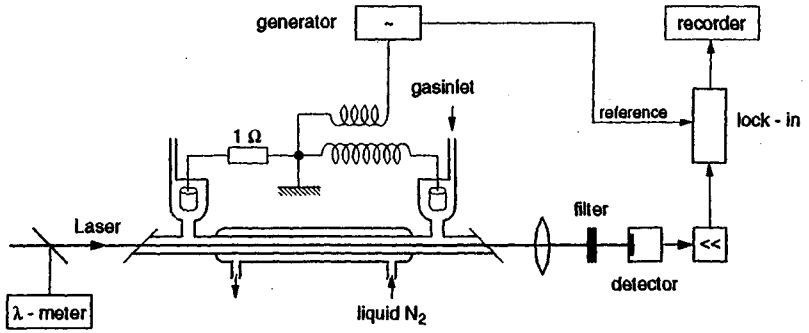


**Fig.6.28.** Experimental arrangement for velocity modulation spectroscopy [6.89]

A typical experimental arrangement [6.90] is depicted in Fig.6.28. With specially designed electron switching circuits polarity modulation frequencies up to 50 kHz can be realized for gas discharges of 300 V and 3 A [6.91]. The attainable signal-to-noise ratio is illustrated by Fig.6.29 which shows the band head of a vibrational band of the $A^2\Pi_{1/2} \leftarrow X^2\Sigma_g^+$ transition of the $CO^+$-ion [6.90].

This technique has been applied first to the infrared region where many vibrational-rotational transitions of ions were measured with colour

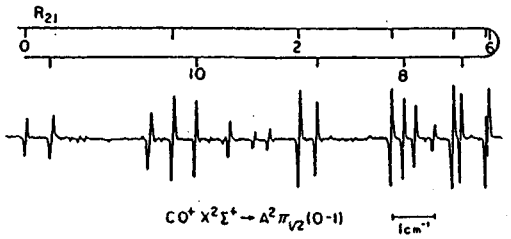


Fig.6.29. Rotational lines around the band head of the $R_{21}$ branch in the $A^2\Pi_{1/2}$ (v' = 1) ← $X^2\Sigma^+$ (v'' = 0) band of $CO^+$ [6.90]

center lasers or diode lasers [6.90,92]. Meanwhile electronic transitions have also been studied with dye lasers [6.93].

A modification of this velocity modulation technique in fast ion beams will be discussed in Sect.9.3.

## 6.7 Laser Magnetic Resonance and Stark Spectroscopy

In all methods discussed in the previous sections of this chapter, the laser frequency $\omega_L$ was tuned across the constant frequencies $\omega_{ik}$ of molecular absorption lines. For molecules with permanent magnetic or electric dipole moments, it is often preferable to tune the absorption lines by means of external magnetic or electric fields across a fixed-frequency laser line. This is particularly advantageous if intense lines of fixed-frequency lasers exist in the spectral region of interest but no tunable source with sufficient intensity is available. Such spectral regions of interest are, for example, the 3÷5 $\mu$m and the 10 $\mu$m ranges, where numerous intense lines of Hf, DF, CO, $N_2O$, and $CO_2$ lasers can be utilized. Since many of the vibrational bands fall into this spectral range, it is often called the *fingerprint* region of molecules.

Another spectral range of interest is the far infrared of the rotational lines of polar molecules. Here a large number of lines from $H_2O$ or $D_2O$ lasers (125$\mu$m) and from HCN lasers (330$\mu$m) provide intense sources. The successful development of numerous optically pumped molecular lasers [6.94] has increased the number of FIR lines considerably.

### 6.7.1 Laser Magnetic Resonance

The molecular level $E_0$ with the total angular momentum J splits in an external magnetic field B into (2J+1) Zeeman components. The sublevel with the magnetic quantum number M shifts from the energy $E_0$ at zero field to



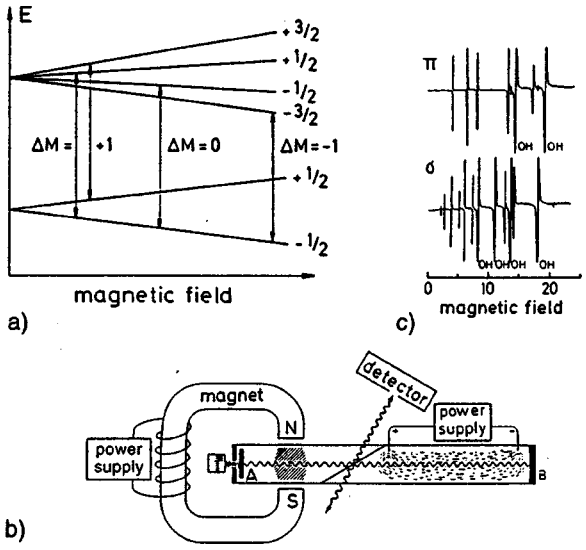


Fig.6.30a,b. Laser magnetic resonance spectroscopy: (a) Level diagram, (b) experimental set-up with an intracavity sample, and (c) LMR spectrum of CH radicals, superimposed by some OH-lines, measured in a low pressure oxygen-acethylene flame with a $H_2O$ laser [6.96]

$$E = E_0 - g\mu_0 BM\,, \tag{6.38}$$

where $\mu_0$ is the Bohr magneton, and g is the Landé factor which depends on the coupling scheme of the different angular momenta (electronic angular momentum, electron spin, molecular rotation, and nuclear spin). The frequency $\omega$ of a transition (v'',J'',M'') → (v',J',M') is therefore tuned by the magnetic field from its unperturbed position $\omega_0$ to

$$\omega = \omega_0 - \mu_0(g'M' - g''M'')B/\hbar \tag{6.39}$$

and we obtain on the transition (v'',J'',M'') → (v',J',M') three groups of lines with $\Delta M = M''-M' = 0, \pm 1$, which degenerate to three single lines if $g'' = g'$ (normal Zeeman effect). The tuning range depends on the magnitude of $g''-g'$ and is larger for molecules with a large permanent dipole moment. These are, in particular, radicals with an unpaired electron, which have a large spin moment. In favorable cases a tuning range of up to 2 $cm^{-1}$ can be reached in magnetic fields of 2 Tesla ($\hat{=}$20KG).

Figure 6.30a explains schematically the appearance of resonances between the fixed frequency $\omega_L$ and the different Zeeman component when the magnetic field B is tuned. The experimental arrangement is illustrated in Fig.6.30b. The sample is placed inside the laser cavity and the laser output is monitored as a function of the magnetic field. The cell is part of a flow system in which radicals are generated either directly in a microwave

discharge or by adding reactants to the discharge close to the laser cavity. A polyethylene membrane beam splitter separates the laser medium from the sample. The beam splitter polarizes the radiation and transitions with either $\Delta M = 0$ or $\pm 1$ can be selected by rotation about the laser axis. For illustration, Fig.6.30c shows the LMR spectrum of the CH radical with some OH lines overlapping. Concentrations of $2 \cdot 10^8$ molecules/cm$^3$ could be still detected with reasonable signal-to-noise ratio for the detector time constant of 1 s [6.95,96].

The sensitivity of this intracavity technique (Sect.6.2.2) can even be enhanced by modulating the magnetic field, which yields the first derivative of the spectrum (Sect.6.2.1). When a tunable laser is used it can be tuned to the center $\nu_0$ of a molecular line at zero field B = 0. If the magnetic field is now modulated around zero the phase of the zero-field LMR resonances for $\Delta M = +1$ transitions is opposite to that for $\Delta M = -1$ transitions. The advantages of this zero-field LMR spectroscopy have been proved for the NO molecule by *Urban* et al. [6.97] using a spin-flip Raman laser.

Because of its high sensitivity LMR spectroscopy is an excellent method to detect radicals in very low concentrations and to measure their spectra with high precision. If a sufficient number of resonances with laser lines can be found, the rotational constant, the fine structure parameters, and the magnetic moments can be determined very accurately. The identification of the spectra and the assignment of the lines are often possible even if the molecular constant have not been known before [6.98]. All radicals observed in interstellar space by radio astronomy have been found and measured in the laboratory with LMR spectroscopy.

Often a combination of LMR spectroscopy with a fixed-frequency laser and absorption spectroscopy at zero magnetic field with a tunable laser is helpful for the identification of spectra.

Instead inside the laser cavity the sample can be also placed outside between two crossed polarizers (Fig.6.31). In a *longitudinal* magnetic field the plane of polarization of the transmitted light is turned, due to the Faraday effect, if its frequency $\omega$ coincides with one of the allowed Zeeman transitions. The detector receives a signal only for these resonance cases while the nonresonant background is blocked by the crossed polarizers [6.99]. This technique is similar to polarization spectroscopy (Sect.7.4). Modulation of the magnetic field and lock-in detection further enhances the sensitivity. In a transverse magnetic field the plane of polarization of the incident beam is chosen 45° inclined against **B**. Due to the Voigt effect the plane of polarization is turned if $\omega_L$ coincides with a Zeeman transition [6.99].

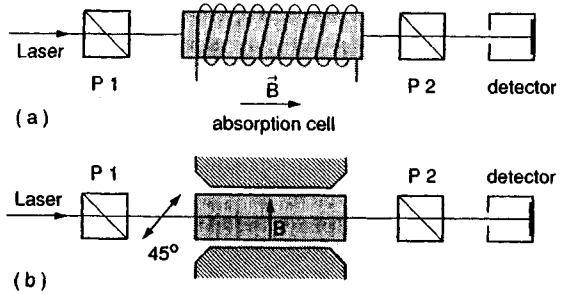


**Fig.6.31.** Schematic arrangement for LMR-spectroscopy using the Faraday-effect in a longitudinal magnetic field (a) or the Voigt-effect in a transverse magnetic field (b) [6.99]

## 6.7.2 Stark Spectroscopy

Analogously to the LMR technique, Stark spectroscopy utilizes the Stark shift of molecular levels in *electric* fields to tune molecular absorption lines into resonance with lines of fixed-frequency lasers. A number of small molecules with permanent electric dipole moments and sufficiently large Stark shifts have been investigated, in particular those molecules which have rotational spectra outside spectral regions accessible to conventional microwave spectroscopy [6.100].

To achieve large electric fields the separation of the Stark electrodes is made as small as possible (typically about 1 mm). This generally excludes an intracavity arrangement because the diffraction by this narrow aperture would introduce intolerably large losses. The Stark cell is therefore placed outside the resonator and for enhanced sensitivity the electric field is modulated while the DC field is tuned. This modulation technique is also common in microwave spectroscopy. The accuracy of $10^{-4}$ for the Stark-field measurements allows a precise determination of the absolute value for the electric dipole moment.

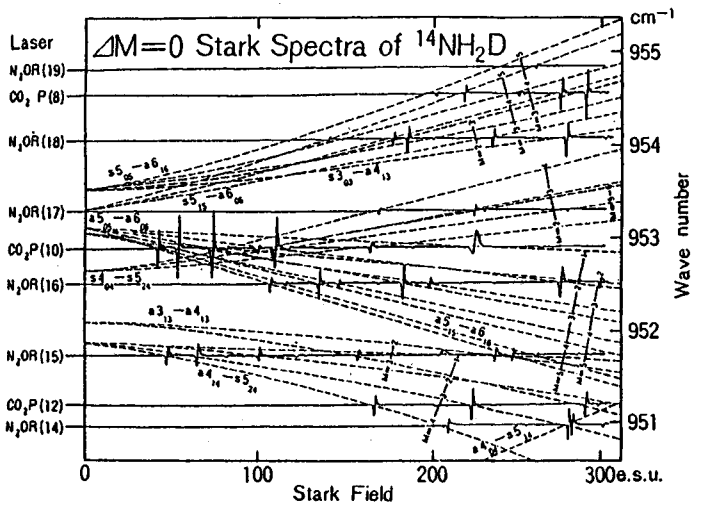


**Fig.6.32.** $\Delta M = 0$ Stark spectra of $^{14}NH_2D$ in the spectral range 950÷955 cm$^{-1}$ obtained with different fixed-frequency laser lines [6.100]

Figure 6.32 illustrates the obtainable sensitivity by a $\Delta M = 0$ Stark spectrum of the ammonia isotope $^{14}NH_2D$ composed of measurements with several laser lines [6.100]. Since the absolute frequency of many laser lines was measured accurately within 20÷40 kHz (Sect.14.7), the absolute frequency of the Stark components at resonance with the laser line can be measured with the same accuracy. The total accuracy in the determination of the molecular parameters is therefore mainly limited by the accuracy of $10^{-4}$ for the electric-field measurements. To date numerous molecules have been measured with laser Stark spectroscopy [6.100-103]. The number of molecules accessible to this technique can be vastly enlarged if tunable lasers in the relevant spectral regions are used, which can be stabilized close to a molecular line with sufficient accuracy and long-term stability.

Stark spectroscopy with constant electric fields and tunable lasers has been performed in molecular beams at sub-Doppler resolution to measure the electric dipole moments of polar molecules in excited vibrational states [6.102].

An efficient way to generate coherent, tunable radiation in the far infrared is the difference frequency generation by mixing the output of an $CO_2$ laser kept on a selected line with the output of a tunable $CO_2$ waveguide laser in a MIM-diode (Sect.5.8). With this technique Stark spectra of $^{13}CH_3OH$ were measured over a broad spectral range [6.103].

Reviews about more recent investigations in LMR and Stark-spectroscopy, including the visible and UV-range, can be found in [6.104-106].

## 6.8 Laser-Induced Fluorescence

Laser-Induced Fluorescence (LIF) has a large range of applications in spectroscopy.

First of all LIF serves as a sensitive monitor for the absorption of laser photons in fluorescence excitation spectroscopy (Sect.6.3.1).

Secondly it is well suited to gain information on molecular states if the fluorescence spectrum excited by a laser on a selected absorption transition is dispersed by a monochromator. The fluorescence spectrum emitted from a selectively populated rovibonric level $(v_k', J_k')$ consists of all allowed transitions to lower levels $(v_m'', J_m'')$ (Fig.6.33). The wave-number differences of these fluorescence lines immediately yield the term differences of those terminating levels $(v_m'', J_m'')$.

A third aspect of LIF is the spectroscopic study of collision processes. If the excited molecule is transferred by inelastic collisions from the level $(v_k', J_k')$ into other rovibronic levels the fluorescence spectrum emitted from these collisionally populated levels gives quantitative information on the collision cross-sections (Sect.13.4).

Another aspect of LIF concerns its application to the determination of the internal-state distribution in molecular reaction products of chemical

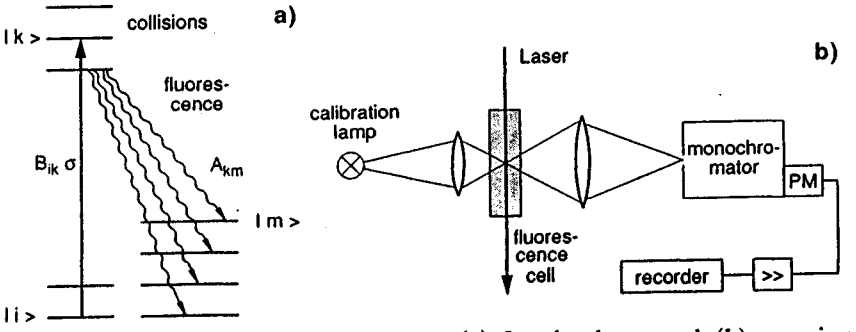


**Fig.6.33a,b.** Laser-induced fluorescence: **(a)** Level scheme and **(b)** experimental arrangement for measuring LIF spectra

reactions (Sects.6.8.4 and 13.6). Under certain conditions the intensity $I_{Fl}$ of LIF excited on the transition $|i\rangle \rightarrow |k\rangle$ is a direct measure of the population density $N_i$ in the absorbing level $|i\rangle$.

Let us now consider some basic facts of LIF in molecules. Extensive information on LIF can be found in [6.107-109].

### 6.8.1 Molecular Spectroscopy by Laser-Induced Fluorescence

Assume a rovibronic level $(v_k', J_k')$ in an excited electronic state of a diatomic molecule has been selectively populated by optical pumping. With a mean lifetime $\tau_k = 1/\Sigma_m A_{km}$ the excited molecules undergo spontaneous transitions to lower levels $E_m(v_m'', J_m'')$ (Fig.6.33). At a population density $N_k(v_k', J_k')$ the radiation power of a fluorescence line with frequency $\nu_{km} = (E_k - E_m)/h$ is given by (Sect.2.6)

$$P_{km} \propto N_k A_{km} \nu_{km} \,. \tag{6.40}$$

The spontaneous transition probability $A_{km}$ is proportional to the square of the matrix element (Sect.2.9)

$$A_{km} \propto \left| \int \psi_k^* \mathbf{r} \psi_m \, d\tau_n \, d\tau_{el} \right|^2 , \tag{6.41}$$

where $\mathbf{r}$ is the vector of the excited electron and the integration extends over all nuclear and electronic coordinates. Within the Born-Oppenheimer approximation [6.110, 111] the total wave function can be separated into a product

$$\psi = \psi_{el} \psi_{vib} \psi_{rot} \tag{6.42}$$

of electronic, vibrational and rotational factors. If the electronic transition moment does not critically depend on the internuclear separation R, the

total transition probability is then proportional to the product of three factors

$$A_{km} \propto |M_{el}|^2 |M_{vib}|^2 |M_{rot}|^2 , \tag{6.43}$$

where the first factor

$$M_{el} = \int \psi'^{*}_{el} r \psi''_{el} d\tau_{el} \tag{6.43'}$$

represents the electronic matrix element which depends on the coupling of the two electronic states. The second integral

$$M_{vib} = \int \psi'_{vib} \psi''_{vib} d\tau_{vib} \quad \text{with} \quad d\tau_{vib} = R^2 dR \tag{6.43''}$$

is the Franck-Condon factor which depends on the overlap of the vibrational wave functions $\psi_{vib}(R)$ in the upper and lower state. The third integral

$$M_{rot} = \int \psi'_{rot} \psi''_{rot} g_i d\tau_{rot} \quad \text{with} \quad d\tau_{rot} = d\vartheta d\varphi \tag{6.43'''}$$

is called the Hönl-London factor. It depends on the orientation of the molecule relative to the electric vector of the incident wave. This is expressed by the factor $g_i$ (i = x, y, z) where $g_x = \sin\vartheta\cos\varphi$; $g_y = \sin\vartheta\sin\varphi$ and $g_z = \cos\vartheta$ [6.110].

Only those transitions for which all three factors are nonzero appear as lines in the fluorescence spectrum. The Hönl-London factor is always zero unless

$$\Delta J = J'_k - J''_m = 0, \pm 1 . \tag{6.44}$$

if a *single* upper level $(v'_k, J'_k)$ has been selectively excited, each vibrational band $v'_k \rightarrow v''_m$ consists of at most *three* lines: a *P line* (J'-J'' = -1), a *Q line* (J'-J'' = 0), and an *R line* (J'-J'' = +1). For diatomic *homonuclear* molecules additional symmetry selection rules may further reduce the number of possible transitions. A selectively excited level $(v'_k, J'_k)$ in a $^1\Pi$ state, for example, emits on a $^1\Pi \rightarrow {}^1\Sigma$ transition either only Q lines or P and R lines, while on a $^1\Sigma_u \rightarrow {}^1\Sigma_g$ transition only P and R lines are allowed [6.111].

The fluorescence spectrum emitted from selectively excited molecular levels of a diatomic molecule is therefore very simple compared with a spectrum obtained under broad-band excitation. Figure 6.34 illustrates this by two fluorescence spectra of the $Na_2$-molecule, excited by two different argon laser lines. While the $\lambda$ = 488 nm line excites a positive $\Lambda$ component in the (v' = 3, J' = 43) level which emits only Q lines, the $\lambda$ = 476.5 nm line populates the negative $\Lambda$ component in the (v'=6, J'=27) level of the $^1\Pi_u$ state, resulting in P and R lines.



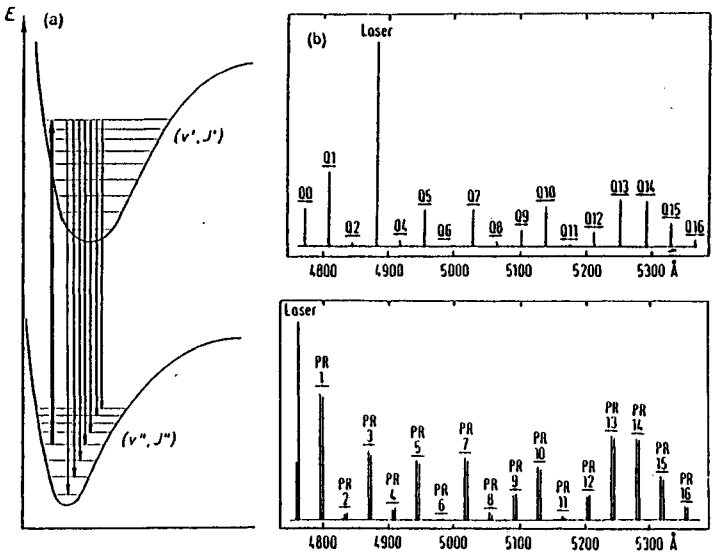


**Fig.6.34.** Laser-induced fluorescence of the $Na_2$ molecule excited by argon laser lines (a) term diagram (b) fluorescence lines with $\Delta J = 0$ (Q-lines) emitted from the upper level (v'=3, J'=43) of the $B^1\Pi_u$ state, excited at $\lambda$ = 488 nm. (c) P and R doublets, emitted from the upper level (v'=6, J'=27)

### 6.8.2 Experimental Aspects of LIF

In atomic physics the selective excitation of single atomic levels was achieved with atomic resonance lines from hollow cathode lamps already before the invention of lasers. However, in molecular spectroscopy only fortituous coincidences between atomic resonance lines and molecular transitions could be used in some cases. Molecular lamps generally emit on many lines and are therefore not useful for the selective excitation of molecular levels.

Tunable narrow-band lasers can be tuned to every wanted molecular transition $|i\rangle \rightarrow |k\rangle$ within the tuning range of the laser. However, selective excitation of a single upper level can only be achieved if neighbouring absorption lines do not overlap within their Doppler width (Fig.6.35). In the case of atoms this can generally be achieved, whereas for molecules with complex absorption spectra, many absorption lines often overlap. In this latter case the laser simultaneously excites several upper levels, which are not necessarily energetically close to each other (Fig.6.35a). In many cases, however, the fluorescence spectra of these levels can readily be separated by a spectrometer of medium size [6.112].

In order to achieve selective excitation of single levels even in complex molecular spectra, one may use collimated cold molecular beams where the Doppler-width is greatly decreased and the number of absorbing levels is

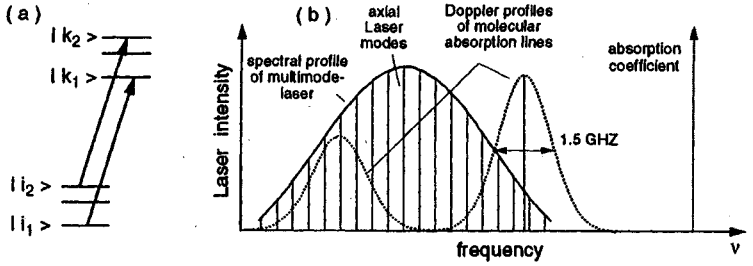


**Fig.6.35a,b.** Doppler-broadened absorption lines overlapping with the spectral line profile of a laser: (a) Level scheme and (b) line profiles

drastically reduced due to the low internal temperature of the molecules (Sect.9.2)

A very elegant technique combines selective laser excitation with high-resolution Fourier-transform spectroscopy of the LIF spectrum. This combination takes advantage of the simultaneous recording of all fluorescence lines and has therefore, at the same total recording time, a higher signal-to-noise ratio. It has meanwhile been applied to the spectroscopy of visible and infrared fluorescence spectra of a large variety of molecules [6.113-115].

When the beam of a single-mode laser passes in the z-direction through a molecular absorption cell only molecules with velocity components $v_z = 0 \pm \gamma$ are excited if the laser is tuned to the center frequency of an absorption line with the homogeneous width $\gamma$. The fluorescence collected within a narrow cone around the z-axis then shows sub-Doppler linewidths which may be resolved with Fourier-transform spectroscopy [6.115].

The advantages of LIF spectroscopy for the determination of molecular parameters may be summarized as follows:

(i) The relatively simple structure of the fluorescence spectra allows ready assignment. The fluorescence lines can be resolved with medium-sized spectrometers. The demands of experimental equipment are much less stringent than those necessary for complete resolution and analysis of absorption spectra of the same molecule. This advantage still remains if a few upper levels are simultaneously populated under Doppler-limited excitation [6.112].

(ii) The large intensities of many laser lines allow achievement of large population densities $N_k$ in the excited level. This yields, according to (6.40), correspondingly high intensities of the fluorescence lines and enables detection even of transitions with small Franck-Condon factors. A fluorescence progression $v'_k \rightarrow v''_m$ may therefore be measured with sufficiently good signal-to-noise ratio up to very high vibrational quantum numbers $v''_m$. The potential curve of a diatomic molecule can be determined very accurately from the measured term energies $E(v''_m, J''_m)$ using the Rydberg-Klein-Rees (RKR) method which is based on a modified WKB procedure [6.116-118]. Since the term values $E(v''_m, J''_m)$ can be immediately determined from the



wave numbers of the fluorescence lines, the RKR potential can be constructed up to the highest measured level $v''_{max}$. In some cases fluorescence progressions are found up to levels $v''$ closely below the dissociation limit [6.120, 121]. This allows the spectroscopic determination of the dissociation energy by an extrapolation of the decreasing vibrational spacings $\Delta E_{vib} = E(v''_{m+1}) - E(v''_m)$ to $\Delta E_{vib} = 0$ (Birge-Sponer plot) [6.122-125].

(iii) The relative intensities of the fluorescence lines $(v'_k, J'_k \rightarrow v''_m, J''_m)$ are proportional to the Franck-Condon factors. The comparison between calculated FCF obtained with the RKR potential from the Schrödinger equation and the measured relative intensities allows a very sensitive test for the accuracy of the potential. In combination with lifetime measurements these intensity measurements yield absolute values of the electronic transition moment $M_{el}(R)$ and its dependence on the internuclear distance R [6.126].

(iv) In several cases discrete molecular levels have been excited which emit continuous fluorescence spectra terminating on repulsive potentials of dissociating states [6.127]. The overlap integral between the vibrational eigenfunctions $\psi'_{vib}$ of the upper discrete level and the continuous function $\psi_{cont}(R)$ of the dissociating lower state often shows an intensity modulation of the continuous fluorescence spectrum which reflects the square $|\psi'_{vib}(R)|^2$ of the upper state wave function (Fig.2.14). If the upper potential is known, the repulsive part of the lower potential can be accurately determined [6.128, 129]. This is of particular relevance for excimer spectroscopy (Sect.5.7) [6.130].

(v) For transitions between high vibrational levels of two bound states the main contribution to the transition probability comes from the internuclear distances R close to the classical turning points $R_{min}$ and $R_{max}$ of the vibrating oscillator. There is, however, a nonvanishing contribution from the internuclear distance R between $R_{min}$ and $R_{max}$, where the vibrating molecule has kinetic energy $E_{kin} = E(v,J) - V(R)$. During a radiative transition this kinetic energy has to be preserved. If the total energy $E'' = E(v',J') - h\nu = V''(R) + E_{kin} = U(R)$ in the lower state is above the dissociation limit of the potential $V''(R)$, the fluorescence terminates in the dissociation continuum (Fig.6.36). The intensity distribution of these "Condon internal diffraction bands" [6.131, 132] is very sensitive to the difference potential $V''(R) - V'(R)$ and therefore allows an accurate determination of one of the potential curves if the other is known [6.133].

### 6.8.3 LIF of Polyatomic Molecules

The technique of LIF is, of course, not restricted to diatomic molecules, but has meanwhile been applied to the investigation of triatomic molecules such as $NO_2$, $SO_2$, $BO_2$, $NH_2$ and many other polyatomic molecules. In combination with excitation spectroscopy it allows the assignment of transitions and the identification of complex spectra. Examples of such measurements have been cited in [6.107-109].

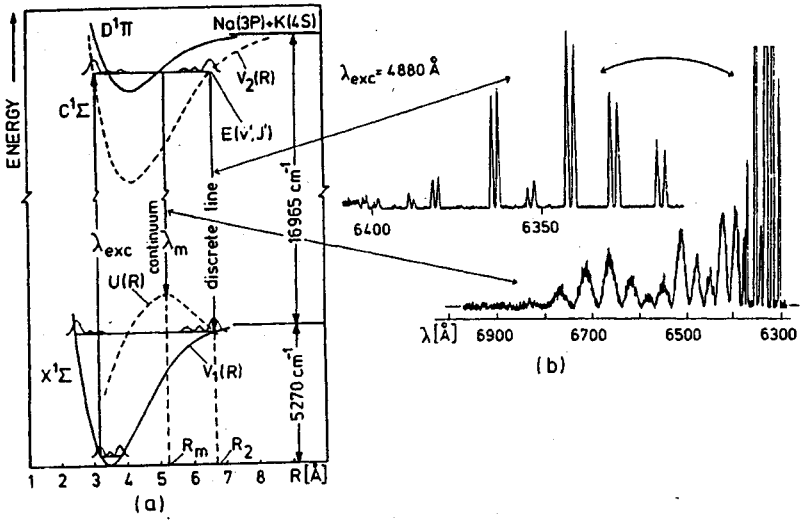


**Fig.6.36.** (a) Schematic potential energy curve diagram illustrating bound-bound transitions between the discrete levels and bound-free transitions from an upper discrete level into the lower continuum above the dissociation energy of the electronic ground state. (b) Two sections of the NaK fluorescence spectrum showing both kinds of transitions [6.131]

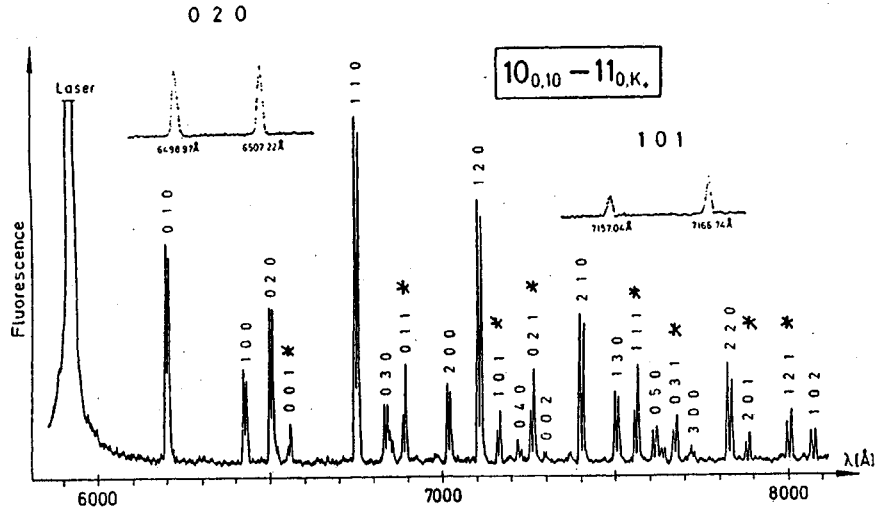


**Fig.6.37.** LIF spectrum of $NO_2$ excited at $\lambda$ = 590.8 nm. The vibrational bands terminating on ground state vibrational levels $(v_1,v_2,v_3)$ marked with an asterix are forbidden by symmetry selection rules but are made allowable by an admixture of a perturbing level with other symmetry to the excited state wave function [6.134]



The LIF of polyatomic molecules opens possibilities to recognize perturbations both in excited and in ground electronic states. If the upper state is perturbed its wave function is a linear combination of the BO wave functions of the mutually perturbing levels. The admixture of the perturber wave function opens new channels for fluorescence into lower levels with different symmetries, which are forbidden for unperturbed transitions. The LIF spectrum of $NO_2$ depicted in Fig.6.37 is an example where the "forbidden" vibrational bands terminating on the vibrational levels $(v_1,v_2,v_3)$ with an odd number $v_3$ of vibrational quanta in the asymmetric stretching vibrational mode in the electronic ground state are marked by an asterix [6.134].

Due to nonlinear couplings between high lying vibrational levels of polyatomic molecules the level structure may become quite complex. The classical motion of the nuclei in such a highly vibrational excited molecule can often no longer be described by a superposition of normal vibrations [6.135]. In such cases a statistical model of the vibrating molecule may be more adequate where the distribution of the energy spacings of neighbouring vibrational levels is investigated. For several molecules a transition regime has been found from *classical oscillations* to *chaotic behaviour* when the vibrational energy is increasing. The chaotic region corresponds to a Wigner distribution of the energy separations of neighbouring vibrational levels. With LIF spectroscopy such high-lying levels in the electronic ground state can be reached. The analysis of such LIF spectra therefore yields information on the dynamics of molecules in vibronically coupled levels [6.136-138].

### 6.8.4 Determination of Population Distributions by LIF

An interesting application of LIF is the measurement of relative population densities $N(v_i'',J_i'')$ and their distribution over the different vibrational-rotational levels $(v_i'',J_i'')$ under situations which differ from thermal equilibrium. Examples are chemical reactions of the type $AB+C \rightarrow AC^*+B$, where a reaction product $AC^*$ with internal energy is formed in a reactive collision between the partners AB and C. The measurement of the internal state distribution $N_{AC}(v'',J'')$ can often provide useful information on the reaction paths and on the potential surfaces of the collision complex $(ABC)^*$. The initial internal state distribution $N_{AC}(v,J)$ is often far away from a Boltzmann distribution. There exist even reactions that produce population inversions allowing the realization of chemical lasers [6.139]. Investigations of these population distributions give important information on the reaction paths and may finally allow the optimization and a better control of these reactions.

The population $N_K(v_K,J_K)$ in the excited states $|k\rangle$ can be determined from the measurement of the fluorescence rate

$$n_{Fl} = N_K A_K V_R \qquad (6.45)$$

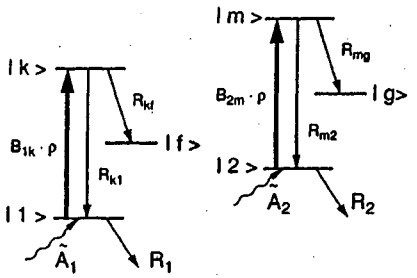


**Fig.6.38.** Level scheme for measurements of population distributions in rotational-vibrational levels of molecular reaction products in their electronic ground state

which represents the number of fluorescence photons $n_{Fl}$ emitted per second from the reaction volume $V_R$.

In order to obtain the population densities $N_i(v_i,J_i)$ in the electronic ground state, the laser is tuned to the absorbing transitions $|i\rangle \rightarrow |k\rangle$ starting from levels $(v''_i,J''_i)$ of the reaction products under investigation and the total fluorescence rate (6.45) is measured for different upper levels $|k\rangle$. Under stationary conditions these rates are according to (3.77) and (6.45)

$$n_{Fl} = N_k A_K V_R = N_i A_K V_R \frac{B_{ik}\rho}{B_{ik}\rho + R_K} \tag{6.46}$$

where $R_K$ is the total (radiative and nonradiative) deactivation rate of the level $|k\rangle$ (Fig.6.38). If the collisional deactivation of level $|k\rangle$ is negligible compared with its radiative depopulation by fluorescence, (6.46) reduces to

$$n_{Fl} = N_i V_R \frac{B_{ik}\rho}{1 + B_{ik}\rho/A_K} . \tag{6.47}$$

We distinguish two limiting cases:

(i) The laser intensity is sufficiently low to ensure $B_{ik}\rho << A_K$. Then the ratio $n_{Fl}(k)/n_{Fl}(m)$ of fluorescence rates observed under excitation of the two transitions $|1\rangle \rightarrow |k\rangle$ and $|2\rangle \rightarrow |m\rangle$ with the same laser intensity $I_L = c\rho$ becomes (Fig.6.38)

$$\frac{n_{Fl}(k)}{n_{Fl}(m)} = \frac{N_1}{N_2}\frac{B_{1k}}{B_{2m}} = \frac{N_1\sigma_{1k}}{N_2\sigma_{2m}} = \frac{\alpha_{1k}}{\alpha_{2m}} \tag{6.48}$$

where $\sigma$ is the optical absorption cross section and $\alpha = N\sigma$ the absorption coefficient. From the measured ratio of fluorescence rates or of absorption coefficients therefore the ratio $N_1/N_2$ of the lower-level population can be obtained if the absorption cross sections are known.



(ii) If the laser intensity is sufficiently high to saturate the absorbing transition we have the case $B_{ik}\rho >> A_K$. Then (6.47) yields

$$\frac{n_{Fl}(k)}{n_{Fl}(m)} = \frac{N_1 A_k}{N_2 A_m} . \tag{6.49}$$

Under stationary conditions the population densities $N_i$ are determined by the rate equations

$$dN_i/dt = 0 = \tilde{A}_i - N_i R_i + \sum_m N_m R_{mi} \tag{6.50}$$

where $\tilde{A}_i$ is the feeding rate of the level $|i\rangle$ by the reaction, or by diffusion of molecules in the level $|i\rangle$ into the detection volume.

$R_i$ is the total deactivation rate of the level $|i\rangle$ whereas $\Sigma N_m R_{mi}$ is the sum of all transition rates from other levels $|m\rangle$ into the level $|i\rangle$.

If $\tilde{A}_i$ is the major term in (6.50), the ratio (6.49) of LIF rates becomes

$$\frac{n_{Fl}(k)}{n_{Fl}(m)} = \tilde{A}_1/\tilde{A}_2 \tag{6.51}$$

and yields directly the ratio of the feeding rates $\tilde{A}_1/\tilde{A}_2$ of the two levels $|1\rangle$ and $|2\rangle$.

First measurements of internal-state distributions of reaction products using LIF have been performed by *Zare* et al. [6.140-142]. One example is the formation of BaCl in the reaction of barium with halogens

$$Ba + HCl \rightarrow BaCl^*(X^2\Sigma^+ v'',J'') + H . \tag{6.52}$$

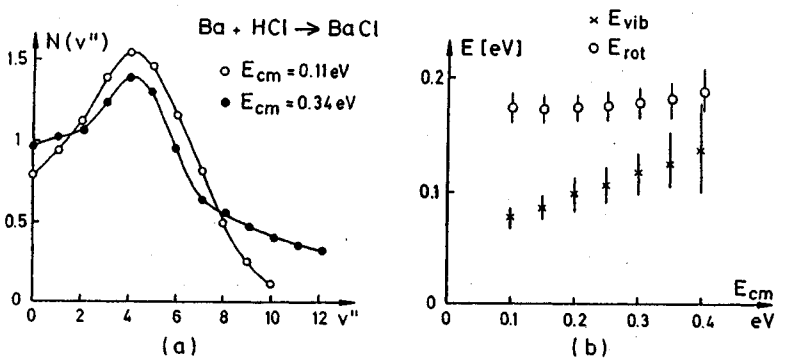


**Fig.6.39.** (a) Vibrational level populations N(v") of BaCl for two different collision energies of the reactants Ba+HCl. (b) Mean vibrational and rotational energy of reactively formed BaCl as a function of the relative collision energy [6.142]

Figure 6.39a exhibits the vibrational population distribution of BaCl for two different collision energies of the reactants Ba and HCl. Figure 6.39b illustrates that the total *rotational* energy of BaCl barely depends on the collision energy in the center of mass system of Ba + HCl, while the *vibrational* energy increases with increasing collision energy.

The interesting question, how the internal state distribution of the products is determined by the internal energy of the reacting molecules, can be answered experimentally with a second laser which pumps the reacting molecule into excited levels (v″J″). The internal state distribution of the product is measured with and without the pump laser. An example which has been studied [6.141] is the reaction

$$Ba + HF(v''=1) \rightarrow BaF^*(v=0 \div 12) + H\,, \qquad (6.53)$$

where a chemical HF laser has been used to excite the first vibrational level of HF and the internal state distrubtion of $BaF^*$ is measured with a tunable dye laser.

Another example is the determination of vibrational-rotational population distributions in supersonic molecular beams [6.143], where molecules are cooled down to rotational temperatures of a few Kelvin (Sect. 9.2).

The method is not restricted to neutral molecules but can also be applied to ionic species. This is of importance when LIF is used for diagnostics of combustion processes [6.144, 145] or plasmas [6.146].

## 6.9 Comparison Between the Different Methods

The different sensitive techniques of Doppler-limited laser spectroscopy, discussed in the previous sections, supplement each other in an ideal way. In the *visible* and *ultraviolet* range, where *electronic* states of atoms or molecules are excited by absorption of laser photons *excitation spectroscopy* is generally the most suitable technique, particularly at low molecular densities. Because of the short spontaneous lifetimes of most excited electronic states $E_k$, the quantum efficiency $\eta_k$ reaches 100% in many cases. For the detection of the laser-excited fluorescence, sensitive photomultipliers are available which allow, together with photon counting electronics (Sect.4.5), the detection of single fluorescence photons with an overall efficiency of $10^{-3} \div 10^{-1}$ (Sect.6.3.1).

Excitation of very high-lying states close below the ionization limit, e.g., by ultraviolet lasers or by two-photon absorption, enables the detection of absorbed laser photons by monitoring the ions. Because of the high collection efficiency of these ions *ionization spectroscopy* represents the most sensitive detection method, superior to all other techniques in all cases where it can be applied.



In the *infrared* region excitation spectroscopy is less sensitive because of the lower sensitivity of infrared photodetectors and because of the longer lifetimes of excited vibrational levels. These long lifetimes bring about either at low pressures a diffusion of the excited molecules out of the observation region or, at high pressures, a collision-induced radiationless deactivation of the excited states. Here *photoacoustic spectroscopy* becomes superior, since this technique utilizes this collision-induced transfer of excitation energy into thermal energy. A specific application of this technique is the quantitative determination of small concentrations of molecular components in gases at higher pressures. Examples are measurements of air pollution or of poisonous constituents in auto-engine exhausts, where sensitivities in the ppb range have been successfully demonstrated.

For infrared spectroscopy in molecular beams opto-thermal spectroscopy is a very good choice (Sect.6.3.3).

For the spectroscopy of atoms or ions in gas discharges, *optogalvanic spectroscopy* (Sect.6.5) is a very convenient and experimentally simple alternative to fluorescence detection. In favorable cases it may even reach the sensitivity of excitation spectroscopy. For the distinction between spectra of ions and neutral species *velocity modulation spectroscopy* (Sect.6.6) offers an elegant solution.

Regarding detection sensitivity, LMR and Stark spectroscopy can compete with the other methods. However, their applications are restricted to molecules with sufficiently large permanent dipole moments to achieve the necessary tuning range. They are therefore mainly applied to the spectroscopy of free radicals with an unpaired electron. The magnetic moment of these radicals is predominantly determined by the electron spin and is therefore several orders of magnitude larger than that of stable molecules in $^1\Sigma$ ground states. The advantage of LMR or Stark spectroscopy is the direct determination of Zeeman or Stark splittings from which the Landé factors and therefore the coupling schemes of the different angular momenta can be deduced. A further merit is the higher accuracy of the *absolute* frequency of molecular absorption lines because the frequencies of fixed-frequency laser lines can be absolutely measured with a higher accuracy than is possible with tunable lasers.

All these methods represent modifications of *absorption* spectroscopy, whereas LIF spectroscopy is based on *emission* of fluorescence from selectively populated upper levels. The absorption spectra depend on both the upper and lower levels. The absorption transitions start from thermally populated lower levels. If their properties are known (e.g. from microwave spectroscopy) the absorption spectra yield information on the *upper* levels. On the other hand, the LIF spectra start from one or a few upper levels and terminate on many rotational-vibrational levels of a lower electronic state. They give information about this lower state.

All these techniques may be combined with intracavity absorption when the sample molecules are placed inside the laser resonator to enhance the sensitivity.

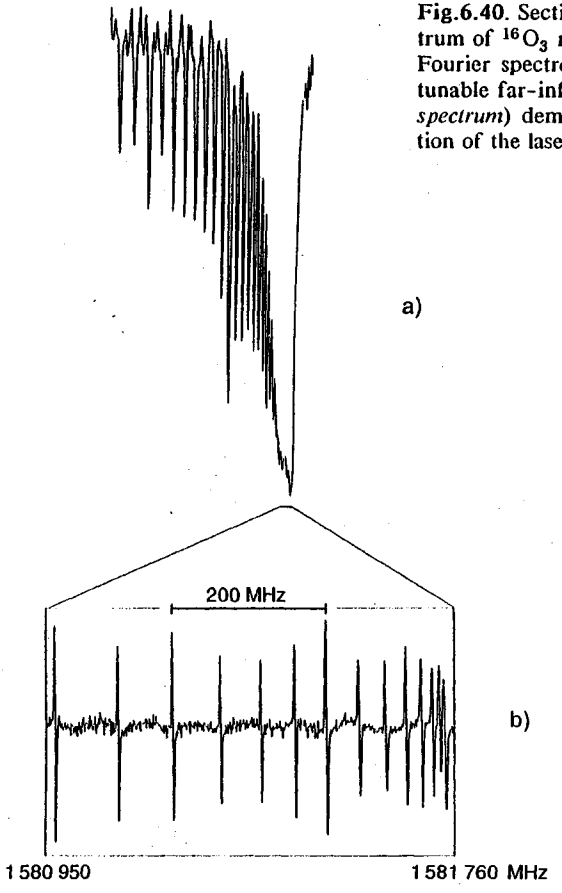


**Fig.6.40.** Section of the pure rotational spectrum of $^{16}O_3$ recorded with a high-resolution Fourier spectrometer (*upper spectrum*) and a tunable far-infrared laser spectrometer (*lower spectrum*) demonstrating the superior resolution of the laser spectrometer [6.147]

A serious competition of laser absorption spectroscopy is Fourier spectroscopy [6.1, 147], which offers the advantage of simultaneous recording of a large spectral interval and with it a short measuring time. In contrast, in laser absorption spectroscopy the whole spectrum must be measured sequentially, which takes much more time. In addition, laser techniques offer the two advantages, namely, a higher spectral resolution and a higher sensitivity. This is demonstrated by examples in two different spectral regimes. Figures 6.40 exhibits part of the submillimeter, purely rotational spectrum of $^{16}O_3$ taken with a high-resolution ($0.003 cm^{-1}$) Fourier spectrometer (a) and a small section of (a) in an expanded scale, recorded with the tunable far-infrared laser spectrometer shown in Figs.4.88 and 5.113. Although the resolution is still limited by the Doppler width of the absorption lines, this imposes here no real limitation because at $\nu = 1.5 \cdot 10^{12}$ Hz the Doppler width of ozon is only $\Delta\nu_D \approx 2$ MHz, compared with a resolution of 90 MHz of the Fourier spectrometer. Another example illustrates the overtone spectrum of $C_2H_2$ around $\lambda = 1.5$ $\mu$m, recorded with a Fourier



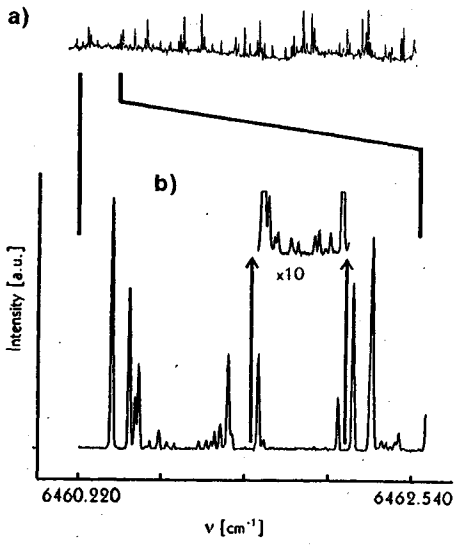


**Fig.6.41.** Comparison of overtone spectra of $C_2H_2$ around $\lambda = 1.5$ $\mu$m, measured (a) with a Fourier spectrometer and (b) with a color-center laser and intracavity optoacoustic spectroscopy [6.45]

spectrometer (Fig.6.41a) and with a colour-center laser and photo-acoustic spectroscopy (b). Weak lines, which are barely seen in the Fourier spectrum, still have a large signal-to-noise ratio in the opto-acoustic spectrum [6.45].